NASA TM X-191

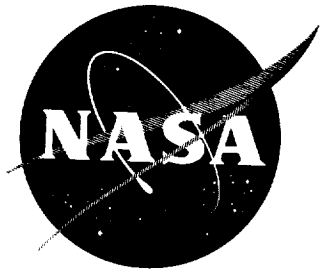

TECHNICAL MEMORANDUM
X-191

HYDRODYNAMIC AND AERODYNAMIC CHARACTERISTICS OF A MODEL OF A SUPERSONIC MULTIJET WATER-BASED AIRCRAFT EQUIPPED WITH SUPERCAVITATING HYDROFOILS

By Robert E. McKann, Ulysse J. Blanchard,
and Albin O. Pearson

Langley Research Center
Langley Field, Va.

Declassified March 15, 1962

NATIONAL AERONAUTICS AND SPACE ADMINISTRATION
WASHINGTON

February 1960

NATIONAL AERONAUTICS AND SPACE ADMINISTRATION

TECHNICAL MEMORANDUM X-191

HYDRODYNAMIC AND AERODYNAMIC CHARACTERISTICS OF A MODEL OF A SUPERSONIC MULTIJET WATER-BASED AIRCRAFT EQUIPPED WITH SUPERCAVITATING HYDROFOILS*

By Robert E. McKann, Ulysse J. Blanchard, and Albin O. Pearson

SUMMARY

The hydrodynamic and aerodynamic characteristics of a model of a multijet water-based Mach 2.0 aircraft equipped with hydrofoils have been determined. Takeoff stability and spray characteristics were very good, and sufficient excess thrust was available for takeoff in approximately 32 seconds and 4,700 feet at a gross weight of 225,000 pounds. Longitudinal and lateral stability during smooth-water landings were good. Lateral stability was good during rough-water landings, but forward location of the hydrofoils or added pitch damping was required to prevent diving.

Hydrofoils were found to increase the aerodynamic lift-curve slope and to increase the aerodynamic drag coefficient in the transonic speed range, and the maximum lift-drag ratio decreased from 7.6 to 7.2 at the cruise Mach number of 0.9. The hydrofoils provided an increment of positive pitching moment over the Mach number range of the tests (0.6 to 1.42) and reduced the effective dihedral and directional stability.

INTRODUCTION

Much effort has been spent in attempts to exploit the potentials of the hydrofoil. In recent years hydrofoils have been applied to boats with considerable success. Most of this work, however, has been done at speeds sufficiently low to avoid cavitation. For the speeds at which water-based aircraft operate, however, cavitation is generally encountered and associated force changes occur which tend to introduce instability in rise and pitch.

*Title, Unclassified.

One solution to the problem of cavitation entails the use of surface-piercing supercavitating hydrofoil sections (ref. 1). Sharp-leading-edge or "supercavitating" hydrofoil sections operating near the water surface tend to ventilate the upper surface of the hydrofoils at low speed and avoid the sudden force changes and severe hydrofoil erosion that generally accompany the onset of cavitation at high speed. Therefore, a supercavitating hydrofoil system has been applied to a supersonic water-based research configuration (ref. 2). Surface-piercing main hydrofoils located ahead of the center of gravity are used in combination with a hard-chine planing afterbody. The functions of strut and lifting surface are combined to obtain a structurally feasible gear. The hydrodynamic characteristics of the configuration with the hydrofoils were investigated in the towing tanks at the Langley Research Center, and the aerodynamic characteristics were determined in the Langley 8-foot transonic pressure tunnel.

The tank investigation was made with hydrofoils installed on the fuselage of the triangular-wing configuration described in reference 2. The resistance, spray, and longitudinal stability during takeoff and landing in smooth water and the motions and angular and vertical accelerations during landings in waves were determined. The longitudinal and lateral stability characteristics were observed during free-body landings in smooth water and in waves. Several longitudinal locations of the hydrofoils and the effect of added pitch damping were investigated.

In order to determine the effect of hydrofoils on the aerodynamic characteristics, wind-tunnel tests were made with hydrofoils installed on the hull of the triangular-wing configuration. These data were obtained to aid in evaluating the need to retract the hydrofoil gear. The longitudinal area distributions of the configuration having a fuselage (ref. 2) or a hull were nearly identical and the aerodynamic characteristics were similar; therefore, the effects of changes in the aerodynamic characteristics of the fuselage due to the addition of the hydrofoils were assumed to be similar to the changes measured with the hydrofoils added to the hull. The lift, drag, and pitching moment were measured over a range of angle of attack at zero yaw and over a range of sideslip for one angle of attack for a Mach number range from 0.6 to 1.42. Yawing moment, rolling moment, and side force were measured over a range of sideslip angles at one angle of attack.

SYMBOLS

Hydrodynamic

A	angular acceleration, radians/sec^2
g	acceleration due to gravity, 32.2 ft/sec^2
h	wave height, ft
l	distance of the hydrofoil trailing-edge tip forward of $\bar{c}/4$, ft
n_v	vertical acceleration, g units
R	total resistance, lb
V	horizontal velocity, knots
V_v	vertical velocity (sinking speed), ft/min
γ	flight-path angle, deg
Δ_o	initial load on water (gross load), lb
δ_s	stabilizer deflection referred to fuselage baseline, positive when trailing edge is down
τ	trim (angle between fuselage baseline and horizontal), deg
τ_L	landing trim (trim at contact), deg

Aerodynamic

All aerodynamic data have been reduced to standard nondimensional coefficients. The wind-tunnel data are referred to the stability-axes system (fig. 1), with the axes originating in the model plane of symmetry at 35 percent of the mean aerodynamic chord in the wing chord plane.

b	wing span, ft
C_D'	drag coefficient, $\frac{\text{Drag}}{qS}$
C_L	lift coefficient, $\frac{\text{Lift}}{qS}$

C_l rolling-moment coefficient, $\frac{\text{Rolling moment}}{qSb}$

C_{l_β} rate of change of rolling-moment coefficient with sideslip angle per degree, $\frac{\partial C_l}{\partial \beta}$

C_m pitching-moment coefficient, $\frac{\text{Pitching moment}}{qS\bar{c}}$

$C_{m_{C_L}}$ rate of change of pitching-moment coefficient with lift coefficient $(C_m \approx 0)$

C_n yawing-moment coefficient, $\frac{\text{Yawing moment}}{qSb}$

C_{n_β} rate of change of yawing-moment coefficient with sideslip angle per degree, $\frac{\partial C_n}{\partial \beta}$

C_Y side-force coefficient, $\frac{\text{Side force}}{qS}$

C_{Y_β} rate of change of side-force coefficient with sideslip angle per degree, $\frac{\partial C_Y}{\partial \beta}$

c chord

$\bar{c}$ wing mean aerodynamic chord, ft

i_t angle of incidence of horizontal tail (-2.5° for these tests), referred to fuselage baseline, deg

L/D lift-drag ratio, $\frac{C_L}{C_D}$

M free-stream Mach number

q free-stream dynamic pressure, lb/sq ft

S wing area, sq ft

α angle of attack of wing chord plane, deg

β angle of sideslip, deg

θ pitching velocity, deg/sec

Subscripts:

max maximum

min minimum

DESCRIPTION OF CONFIGURATION

The basic configuration with a fuselage and hydro-ski gear has been described in reference 2. The general arrangement of the configuration with a fuselage and a hydrofoil gear is shown in figure 2. All mission and performance characteristics were assumed to be the same as those described in reference 2, and all major components of the aircraft were retained with the exception of the hydro-ski gear, which was replaced by a hydrofoil gear.

A pair of supercavitating hydrofoils was extended downward from the bottom on either side of the fuselage at a negative dihedral of 45° in order to provide hydrodynamic lifting surfaces which would permit the fuselage to run above the water and avoid wave impacts and hydrodynamic resistance at high speeds. Location of the hydrofoils near the center of gravity is desirable to avoid large hydrodynamic pitching moments from the hydrofoils, especially during operation at high speed in waves.

Preliminary rough-water taxi tests of a 1/20-size tank model were made with a pair of triangular-plan-form (no trailing-edge sweepback) hydrofoils having an aspect ratio of 2.56. The aerodynamic tests also were made with these hydrofoils. The preliminary tank tests in rough water indicated that the vertical accelerations resulting from wave impacts were relatively large, as were the motions in pitch and rise. Increasing the aspect ratio of the hydrofoils from 2.56 to 3.54 by increasing the span, decreasing the root chord, and making a finite tip chord resulted in a marked improvement in the rough-water behavior; therefore, the present tank tests were made with the altered hydrofoils which had a taper ratio of 0.10. The characteristic dimensions of the low-aspect-ratio hydrofoils used for the aerodynamic investigation and of the hydrofoils having a higher aspect ratio used for the tank tests are given in table I in terms of full-size dimensions.

MODELS

Tank Model

Photographs of the 1/14-size dynamic tank model are presented in figure 3. A similar 1/20-size model was used for preliminary rough-water and free-body tests. The 1/14-size model was required to permit smooth- and rough-water tests on the towing carriage at gross weights corresponding to the takeoff (design gross weight) and the landing condition (two-thirds of the design gross weight) at a scale takeoff speed which was within the speed capability of the towing carriage.

The fuselages were constructed of plastic-impregnated glass cloth, wood, and aluminum. The wing was of solid balsa and hardwood construction covered with a thin plastic-impregnated glass-cloth skin. Tail surfaces were of conventional wooden construction covered with silk. The hydrofoils and their associated attachment devices were made of aluminum.

The wing incidence was fixed at 10° (relative to the fuselage baseline), and leading-edge slats were used to prevent premature wing stall usually encountered at the low Reynolds numbers of the tank tests. The all-movable, horizontal-tail surfaces were provided with a linkage system to give an elevator-stabilizer deflection ratio of approximately 2 to 1 over a stabilizer deflection range from 10° to -15°. Because of the low aerodynamic pitch damping inherent in this configuration, the effect of additional aerodynamic damping on the hydrodynamic characteristics was investigated. The damping was provided by a gyro-controlled elevator actuator, shown in figure 4 and described in reference 3.

The hydrofoils were cut from flat-aluminum stock and were welded to attaching plates at the root. The leading-edge bevel of 9° was machined, and the assembly was anodized. A flat hydrofoil section was used for simplicity of construction, since preliminary test results, shown in figure 5, indicated no significant change in resistance at low speeds from that of a circular-arc cambered section. Some decrease in the trim and rise and an increase in the emergence speed were accepted.

A sealed compartment was built into the bottom of the fuselage forward of the center of gravity and was equipped with mounting tracks for internal attachment of the hydrofoils. The tracks facilitated hydrofoil-configuration changes, fore-and-aft positioning, or hydrofoil-incidence changes. The compartment was sealed by lightweight slotted hatches and tape, thus providing a faired fuselage hydrofoil intersection. Preliminary tests with the 1/20-size model had indicated no fuselage or hydrofoil spray near the forward engine inlets. In order to save weight, the forward engine nacelles were not included on the 1/14-size model.

Electric contacts were located on the hull keel at the bow and stern and at the hydrofoil tips. The contacts indicated when these parts of the model were in contact with the water and also were used to release a trim brake during landing tests.

Wind-Tunnel Model

Photographs of the 1/42.5-size wind-tunnel model of the hull configuration with the hydrofoils are shown in figure 6. The fuselage was of plastic-impregnated glass cloth over a steel core in which the six-component strain-gage balance was housed. The aerodynamic surfaces and forward nacelles and struts were of stainless steel. The rear nacelles were of plastic-impregnated glass cloth. The rear portion of the fuselage was cut off to allow installation of the support sting.

The triangular-plan-form hydrofoils were made from flat stainless steel with a 9° bevel on the upper surface at the leading edge. They were attached to the hull bottom at a fixed incidence of 9° relative to the fuselage baseline. The characteristics and dimensions of the hydrofoil system are given in table I.

APPARATUS AND PROCEDURE

Hydrodynamic Investigation

General.- The hydrodynamic investigation was made in the towing tanks at the Langley Research Center. The apparatus and procedures used are generally similar to those described in references 4 and 5. The model is shown on the towing apparatus in figure 7, and the catapult for the free-body tests is shown in figure 8.

All tests were made with the center of gravity located at $\bar{c}/4$, a wing incidence of 10°, and a hydrofoil incidence (measured relative to the fuselage baseline in the vertical plane) of 9°. Smooth-water resistance and takeoff tests were made at a model weight corresponding to 225,000 pounds (full size), and landing tests on the towing carriage were made at a model weight which corresponded to a full-size weight of 150,000 pounds. Catapult landings were made at a weight corresponding to a weight of 160,000 pounds. Engine thrust was not simulated during any of the tests; however, the unbalanced moment in pitch due to thrust was simulated for the takeoff tests by a weight moment applied to the model. Landings were assumed to be power-off and no thrust moment was simulated.

Spray characteristics in smooth water and in waves were determined from visual observations, photographs, and motion pictures. Smooth-water spray was studied during constant-speed and accelerated runs to takeoff and during landing tests. Spray characteristics in waves were determined during landings and constant-speed taxi runs.

Smooth-water tests.- For the tests on the towing carriage in smooth water, the model was pivoted at the center of gravity and had freedom in only trim and rise. The longitudinal forces (resistance and drag) were obtained by means of a mechanical optical dynamometer connected to the towing gear. At the design gross weight the trim, rise, and resistance, including air drag of the complete model, were obtained for a range of constant speeds for several fixed stabilizer deflections with the thrust moment simulated. ("Rise" is defined as the distance of the tips of the hydrofoils from the undisturbed water surface, being positive when the hydrofoils are above the water surface and zero when they contact the undisturbed water at zero trim.) Trim and rise were also measured during accelerated runs $\left(4\frac{1}{2}\ \text{ft/sec}^2\right)$ to takeoff for a range of fixed stabilizer deflections.

Landings were made in smooth water over a range of contact trims. With the model held at the desired landing trim by the trim brake, the carriage was decelerated at a uniform rate from a speed in excess of flying speeds, thus allowing the model to glide onto the water. At the instant of model contact with the water surface the trim brake was automatically released to allow a free-to-trim landing runout. Time histories of speed, trim, and rise were recorded.

Rough-water tests.- For rough-water tests on the towing carriage, the model had fore-and-aft freedom in addition to freedom in trim and rise. The landings were made by using the same procedure as for smooth-water landings. Landings were made at a landing trim of 10° and were primarily in waves 4 feet high over a range of wave lengths from 160 to 420 feet. A minimum of 8 landings in each wave length was made whenever possible. A few landings were made in 2- and 6-foot waves. Three hydrofoil longitudinal positions were investigated. Artificial pitch damping in which a gearing ratio $\left(\text{ratio of elevator deflection to pitching velocity } \frac{\partial \delta_s}{\partial \dot{\theta}}\right)$ of 2.37 seconds was provided for most of the rough-water landings. Only in the most forward hydrofoil positions were landings made without pitch damping as well as with pitch damping. Time histories of speed, trim, fore-and-aft position of the model, horizontal-tail deflections, and vertical and angular accelerations were recorded.

Vertical accelerations were measured with a strain-gage accelerometer mounted on the towing staff. The angular accelerations were measured with a matched pair of accelerometers of the same type located within the model. In the static condition all accelerometers were considered to read zero. The frequency-response curves of the strain-gage-accelerometer and

recording-galvanometer systems were flat to within ±5 percent between 0 and 27 cycles/sec, as in previous tests.

Because of inherent model structural vibration during rough-water landings, the accelerometer traces had to be faired in order to obtain the impact-loads data. Figure 9 shows the record of the accelerometer traces for a typical landing. The method used to fair the vibrations is also indicated. The envelope of the vibration is estimated and the mean axis of the envelope is drawn to aid in obtaining the transient load. Consideration is given to the duration of the initial oscillation and to the rate of change of model displacement in fairing the accelerometer traces. The envelope method of waveform analysis described in reference 6 was used in fairing the envelope of the structural vibration.

Free-body landings.- Free-body landings were made with the 1/20-size model by using the catapult shown in figure 8. The catapult consisted mainly of a "sling-shot" propulsive unit made up of rubber-strand shock cords, pulleys, and cables, a pair of rails and supporting structure, and a launching carriage. The model was supported at the desired landing attitude by a three-point, zero-length launching arrangement which allowed it to be cast free when the carriage encountered the arrester cords (bumper) near the forward end of the rails. The model was statically balanced and the elevators were set to maintain the launching attitude during free glide onto the water.

The free-body landings were made in smooth water and in waves at a weight corresponding to 160,000 pounds and with the hydrofoils in the aft and intermediate longitudinal positions (l = 3.0 and 6.3 feet, respectively). The landings were made with fixed controls at a landing trim of 9° and with initial zero roll and zero yaw. The speed at launching was the minimum flight speed. Visual observations and motion-picture cameras were used to determine landing behavior.

Aerodynamic Investigation

The aerodynamic investigation was conducted in the Langley 8-foot transonic pressure tunnel with natural transition on the model at Mach numbers from 0.6 to 1.42. Reynolds number based on $\bar{c}$ varied between 1.0×10^6 and 1.25×10^6 over the Mach number range of the tests.

The tunnel has a slotted test section in which the Mach number can be varied continuously to a Mach number of 1.2. Fairings which were described in reference 7 were used to enclose the slots of the test section to produce a Mach number of 1.42. All aerodynamic data presented are essentially free of wall-reflected disturbances. The present investigation was conducted at a stagnation pressure of 0.5 atmosphere and at a dewpoint such that the air flow was free of condensation shocks.

Measurements.- The model was mounted on a sting-supported, six-component strain-gage balance as shown in figure 6. The force and moment results have been adjusted to the condition of free-stream static pressure on the base of the model. In addition, the internal drag has been subtracted from the drag data to give a net external drag. The internal drag values used are given in reference 2.

The angle of attack of the model was varied from about -4° to 16°. Characteristics in sideslip of the model with the hydrofoils were obtained at angles of sideslip from -4° to 8° at an angle of attack of approximately 5°. The angles of attack and yaw have been corrected for balance and sting deflections and for stream-flow angularity.

Accuracy.- Based on balance calibrations and repeatability of data, it is estimated that the various measured quantities are accurate to within the following limits:

Mach number	±0.005
α, deg	±0.1
β, deg	±0.1
C_L	±0.03
C_D'	±0.002
C_m	±0.010
C_l	±0.0013
C_n	±0.0038
C_Y	±0.03

RESULTS AND DISCUSSION

Hydrodynamic

Smooth-water spray.- Typical photographs of the smooth-water-spray characteristics are shown in figure 10. Forward spray was very light, and it is evident from the photographs that the forward nacelle location would be well clear of spray at all times. The rear nacelle inlets were free from spray at all speeds, but light spray impinged upon the aft end of the nacelle at speeds between 100 and 160 knots. The horizontal-tail surfaces were clear of spray, and only light wetting of the lower wing surface occurred at low speed (approximately 45 knots, full size).

Spray from the upper surface of the hydrofoils tended to remain outboard of the fuselage and below the wing and did not significantly affect the behavior of the model. Spray from the lower surface of the hydrofoils concentrated in the area between and behind the

hydrofoils and rose sharply to strike the fuselage a short distance aft of the hydrofoils at low speeds. The local flow around a similar hydrofoil is illustrated in figure 11. As the speed increased, the spray from the hydrofoils moved back along the fuselage and decreased in quantity but increased in velocity relative to the model.

Smooth-water resistance.- The total resistance and corresponding trim and rise for several stabilizer deflections are presented in figure 12. In the speed region between 20 and 40 knots, the model trim and rise increased rapidly as the hydrofoils lifted the model. At constant speed between 30 and 35 knots, a nondivergent oscillation in trim and rise occurred. During these oscillations the model trimmed up until the condition was reached for separation of the flow (venting) from the upper surface of the hydrofoils. The resulting loss of lift by the hydrofoils caused the rise and trim to decrease. The flow again attached to the upper surface of the hydrofoil and the cycle was repeated. During takeoff runs the model accelerated through this region with no instability.

After the initial rapid increase in trim and rise at 30 knots, the model continued to rise at a much slower rate as speed was increased to takeoff. In the speed region from 40 to 60 knots, the trim remained nearly constant as a result of the nearly equal balance between the lift of the hydrofoils forward and the lift on the afterbody due to the roach from the hydrofoils. Between 60 and 90 knots, the trim decreased principally because of the lift on the afterbody produced by the hydrofoil roach. Photographs in figure 10 show that in this speed range the entire forebody was clear of the spray, but the heavy roach from the underside of the hydrofoils rose steeply to strike the afterbody. The roach and the drag of the hydrofoils apparently combined to produce the undesirable low trim in a speed region where the elevators were relatively ineffective. The total resistance rose to a maximum value in this region and resulted in a minimum gross-load—total-resistance ratio of 2.4 at a speed of about 75 knots. Above this speed the resistance fell off sharply. Low-amplitude, low-frequency trim oscillations occurred at about 80 knots.

At speeds above 100 knots, the elevators became effective and it was possible to reduce the resistance by decreasing the trim to values corresponding more nearly to those for $(L/D)_{max}$ of the hydrofoils and aerodynamic surfaces. In addition, the resistance decreased because of a marked reduction in afterbody wetting.

Excess thrust for acceleration was available throughout the speed range for takeoff. A takeoff could be made in approximately 32 seconds and 4,700 feet in smooth water.

Takeoff stability.- The variation of trim with speed during accelerated runs simulating takeoff for several fixed-stabilizer deflections

is shown in figure 13. In general, the characteristics of the trim tracks for the range of stabilizer deflections were very similar. The takeoff stability was very good and the trim oscillations which occurred between 70 and 90 knots were considered insignificant. The rise instability experienced at low speeds during constant-speed resistance tests was not evident during accelerated takeoff. The range of fixed-stabilizer deflections for takeoff extended from -6° to -15°.

Landing stability in smooth water.- Figure 14 presents typical variations in trim and rise with speed during landings in smooth water. Except for the initial trim oscillation, which was dependent upon landing trim, subsequent trim oscillations were relatively mild and quickly damped. Rise oscillations also were highly damped.

The maximum variations in trim and rise, during the greatest cycle, as well as the number of rebounds during landings in smooth water are presented in figure 15 as indicated by the rebounds at contact trims of 5.6° and 5.8°. An uncorrected variation of the height of the hydrofoil tip with trim results in a small negative rise reading when the model is actually clear of the water. The maximum amplitude of trim and rise did not vary significantly through the range of landing trims. Landing stability was considered very good. Lateral stability during free-body landings was satisfactory.

Landings in waves.- The data obtained during landings in waves with and without the addition of pitch damping are presented in full-size values in table II. This table contains the pertinent information regarding the impacts which produced the maximum vertical and angular accelerations for the various conditions investigated.

Figure 16 shows the variation with wave length of maximum vertical acceleration, maximum angular acceleration, and the maximum and minimum values of the trim during the greatest trim cycle and of rise during the greatest rise cycle in the landing in waves 4 feet high. The variation of impact loads and motions with wave length was small and the overall maximum hydrodynamic load experienced for all conditions tested in 4-foot waves was approximately 3.4g. The usual experience for seaplanes to have greater positive than negative angular accelerations during landings in waves was reversed for this configuration, as indicated in figure 16. This difference is further evidence of the influence of the hydrofoil wake on a relatively strong afterbody.

The effect of wave height on the loads and motions is shown in figure 17, in which the data for three wave heights at one wave length are plotted. Vertical accelerations increased greatly with increase in wave height from 2 to 6 feet. The positive (bow-up) angular accelerations increased rapidly in waves greater than 4 feet in height as a result of

the forebody contacting the waves at higher speeds. With increased wave height, trim amplitudes increased and the minimum trims were lower so that in 6-foot waves the bow began to plow. Rise amplitudes also increased with increasing wave height and the model began leaving the water in 6-foot waves.

The effect of hydrofoil longitudinal position on the landing loads and motions in waves is summarized in figure 18, in which the maximum loads and motions for three wave lengths (from the faired data of fig. 16) are presented. There is little change in maximum loads and motions over the range of wave lengths tested except for rise, where there is a tendency to increase amplitude with increase in wave length as the hydrofoils are moved forward. Although the maximum values of trim motion show little change, significant changes in trim motion at high speed occurred with change in hydrofoil longitudinal position as illustrated in figure 19, which shows time histories of trim motions taken from several oscillograph records of landings with the hydrofoils in the most aft position (l = 3.0 feet) and in the intermediate position (l = 6.3 feet). It can be seen that the trim oscillations were milder during the early portion of the landings for the most aft position; however, the model assumed very low trim attitudes at high speeds. These low trim attitudes looked rather dangerous in waves and, during free-body landings that were made without pitch damping, the model occasionally tripped and dived. However, with the hydrofoils in the intermediate position, no diving occurred and the lateral stability was good.

A further illustration of the effect of longitudinal position of the hydrofoils is shown by typical oscillograph records for the aft (fig. 20(a)) and intermediate (fig. 20(b)) positions. As in figure 19, trim motions and maximum trim values were less at high speed with the hydrofoils in the aft position, and the model was observed to run almost entirely on the hydrofoils with the afterbody relatively clear. This accounts for the reduced motions in trim and rise and the reduced loads noted in figure 20(a) for this speed region. With the hydrofoils moved forward, the model ran on the hydrofoils and the afterbody at high speed, thus resulting in more severe loads in this speed region. Loads and motions for this configuration might be improved by providing increased afterbody clearance and a rear lifting surface with rough-water capabilities similar to those demonstrated by the hydrofoils.

The effect of added pitch damping is shown by typical time histories in figure 21. With fixed controls (gyro off), the trim oscillations were larger and persisted throughout the landing run. It should be noted in particular that undesirably low trims occurred at high speeds even for this forward hydrofoil position when the controls were fixed. With added pitch damping, more desirable trim attitudes were maintained throughout the landing run and the motions were well damped. These effects were

true for all wave lengths tested (fig. 16). The loads and rise characteristics were relatively unchanged by added pitch damping.

Rough-water spray.- Spray characteristics in rough water were satisfactory. In general, spray was concentrated aft of the wing and the forward engines would be well clear in all waves tested. In the 6-foot waves, some loose fine spray entered the aft inlets.

Aerodynamic

Longitudinal aerodynamic characteristics.- The variation of angle of attack, drag coefficient, and pitching-moment coefficient with lift coefficient over the Mach number range from 0.6 to 1.42 for the hull version of the present configuration without hydrofoils and with hydrofoils is shown in figure 22. The longitudinal aerodynamic characteristics are summarized in figure 23.

The installation of the hydrofoils appears to have had little effect on the linearity of the lift coefficient with angle of attack. The lift-curve slope was increased by approximately 0.01 at $M = 1.0$ but only slightly at $M = 0.6$ or 1.42.

The hydrofoils increased the minimum drag coefficient throughout the Mach number range, and the increment in minimum drag coefficient was greatest near $M = 1.0$. The drag-rise Mach number $\left(\text{defined as } \frac{dC_D'}{dM} = 0.1\right)$ was decreased from 0.96 to 0.94 by the addition of the hydrofoils.

A plot of the maximum lift-drag ratio indicates that the addition of the hydrofoils resulted in a decrease in the overall aerodynamic efficiency from 7.6 to 7.2 at $M = 0.9$ (fig. 23).

The hydrofoils provided an increment of positive (nose-up) pitching-moment coefficient which increased with increasing lift coefficient over the Mach number range. This increment in pitching-moment coefficient would be expected since the hydrofoils were located forward of the center of gravity. No pitchup tendency was noted. The hydrofoils produced a somewhat greater rearward shift of the aerodynamic center ($0.19\bar{c}$ as compared with $0.17\bar{c}$) over the Mach number range but resulted in a more forward location of the aerodynamic center for all speeds of the test.

Lateral aerodynamic characteristics.- The force and moment coefficients with the hydrofoils are shown for a range of sideslip angles at an angle of attack of approximately 5.0° in figure 24. Data for the basic configuration were not available for comparison. The lateral

force and moment characteristics are linear over most of the sideslip range of the test.

The lateral stability parameters of the hull model with and without hydrofoils are summarized in figure 25. The addition of the hydrofoils reduced the positive effective dihedral and directional stability while introducing a large increment of C_{Y_β} over the Mach number range.

CONCLUDING REMARKS

The hydrodynamic and aerodynamic characteristics of a model of a multijet water-based aircraft capable of supersonic speeds and equipped with surface-piercing supercavitating hydrofoils have been investigated. The minimum gross-load—total-resistance ratio on the water was 2.4, and sufficient excess thrust was available for a takeoff in approximately 32 seconds and 4,700 feet in smooth water. Longitudinal stability during smooth-water takeoff and landing was considered very good. Overall inlet, tail, and wing spray clearances were good. The afterbody bottom and sides were heavily wetted by the wake from the lower surface of the hydrofoils.

With added aerodynamic pitch-damping control, maximum impact loads and motions in 4-foot waves did not vary appreciably with wave length and hydrofoil longitudinal position, although the most aft hydrofoil position exhibited undesirably low trim attitudes at high speeds. This added aerodynamic pitch-damping control was considered necessary to prevent possible diving during rough-water operation except for the most forward hydrofoil longitudinal position. Added pitch damping did not affect maximum impact loads appreciably but reduced undesirable trim motions. Spray characteristics in rough water were satisfactory. Directional and lateral stability in smooth and rough water were good during free-body landings.

The hydrofoils were found to increase the lift-curve slope in the transonic speed region, but they also increased the drag coefficient, thus resulting in a reduction in the maximum lift-drag ratio from 7.6 to 7.2 at the cruise Mach number of 0.9. The drag-rise Mach number was decreased from 0.96 to 0.94 by the addition of the hydrofoils. The hydrofoils provided an increment of positive pitching moment over the Mach number range of the tests, 0.6 to 1.42, and reduced the effective dihedral and directional stability. The addition of the hydrofoils produced a somewhat greater rearward shift of the aerodynamic center ($0.19\bar{c}$ as compared with $0.17\bar{c}$ where $\bar{c}$ denotes the wing mean aerodynamic chord)

over the Mach number range but resulted in a more forward location of the aerodynamic center for all speeds of the test.

Langley Research Center,
National Aeronautics and Space Administration,
Langley Field, Va., August 28, 1959.

REFERENCES

1. Tulin, M. P., and Burkart, M. P.: Linearized Theory for Flows About Lifting Foils at Zero Cavitation Number. Rep. C-638, David W. Taylor Model Basin, Navy Dept., Feb. 1955.

2. Petynia, William W., Hasson, Dennis F., and Spooner, Stanley H.: Aerodynamic and Hydrodynamic Characteristics of a Proposed Supersonic Multijet Water-Based Hydro-Ski Aircraft With a Variable-Incidence Wing. NACA RM L57G05, 1957.

3. Schade, Robert O., and Hassell, James L., Jr.: The Effects on Dynamic Lateral Stability and Control of Large Artificial Variations in the Rotary Stability Derivatives. NACA Rep. 1151, 1953. (Supersedes NACA TN 2781.)

4. Olson, Roland E., and Land, Norman S.: Methods Used in the NACA Tank for the Investigation of the Longitudinal-Stability Characteristics of Models of Flying Boats. NACA Rep. 753, 1943. (Supersedes NACA WR L-409.)

5. Parkinson, John B.: NACA Model Investigations of Seaplanes in Waves. NACA TN 3419, 1955.

6. Manley, R. G.: Waveform Analysis. John Wiley & Sons, Inc. (New York), 1945.

7. Wright, Ray H., and Ward, Vernon G.: NACA Transonic Wind-Tunnel Test Sections. NACA Rep. 1231, 1955. (Supersedes NACA RM L8J06.)

TABLE I

DIMENSIONS AND CHARACTERISTICS OF THE HYDROFOIL SYSTEMS

[All values are full size]

Characteristics	Tank model	Wind-tunnel model
Number of hydrofoils	2	2
Hydrofoil section	(a)	(a)
Leading-edge sweepback, deg	37.5	37.5
Trailing-edge sweepback, deg	20	0
Total surface area, sq ft	153.2	183
Total projected area, sq ft	108.4	128
Aspect ratio, surface area	3.64	2.56
Aspect ratio, projected area	2.57	1.82
Taper ratio	0.10	0
Dihedral, deg	-45	-45
Incidence, deg	9	9
Ratio of gross weight to total projected area, lb/sq ft	2,076	1,758
Distance of tip below fuselage baseline, ft	11.5	8.0
Distance of trailing edge at tip ahead of wing $\bar{c}/4$, ft	3.0, 6.3, 8.6	6.3
Average sternpost angle, deg	9.1	-----

[a]Rectangular with 9° leading-edge chamfer on upper surface.

TABLE II

DATA OBTAINED DURING LANDINGS IN WAVES

[All values are full size; initial landing trim, ≈10°]

(a) l = 3.0 feet; with aerodynamic pitch damping

Landing	Wave height, ft	Wave length, ft	τ_L, deg	V_v, ft/min	V, knots	γ, deg	n_v, g units	A, radians/sec^2
1	2	210	9.9	287	59.4	2.7	1.2	---
2			9.9	402	131.1	[illegible].7	1.0	---
3			10.0	258	67.1	2.2	1.1	---
4			10.2	242	62.5	2.2	.9	---
5	4	210	10.0	608	52.1	6.6	2.3	---
6			10.0	523	63.3	[illegible].7	2.4	---
7			10.1	674	62.0	[illegible].4	2.8	---
8			10.1	705	49.8	7.9	2.6	---
9	4	252	9.8	617	60.0	[illegible].8	2.6	---
10			9.9	817	45.9	[illegible].9	2.3	---
11			9.8	599	58.3	[illegible].8	2.4	---
12			9.9	678	62.0	6.2	2.8	---
13			9.9	541	63.1	4.9	2.2	---
14			9.9	570	63.8	5.0	2.4	---
15			9.9	597	56.7	5.9	2.2	---
16			9.9	707	52.3	7.6	2.1	---
17	6	210	9.8	694	84.8	4.6	4.4	3.6
18			9.8	880	95.2	5.2	4.5	2.7
19			9.8	824	98.8	4.7	4.2	2.3
20			9.8	988	79.3	7.0	4.6	4.6
21			9.8	546	71.3	4.3	3.6	2.1
22			9.8	573	84.2	3.8	3.4	2.9
23			9.8	604	75.3	4.5	3.6	1.6
24			9.8	844	83.5	5.7	4.3	3.6

TABLE II.- Continued

DATA OBTAINED DURING LANDINGS IN WAVES

[All values are full size; initial landing trim, ≈10°]

(b) l = 6.3 feet; with aerodynamic pitch damping

Landing	Wave height, ft	Wave length, ft	τ_L, deg	V_v, ft/min	V, knots	γ, deg	n_v, g units	A, radians/sec^2
1	2	252	9.7	337	70.4	2.7	1.1	0.5
2			9.7	240	83.9	1.6	1.1	.5
3			9.7	305	81.7	2.1	1.2	.5
4			9.7	308	82.0	2.1	1.0	.7
5			9.7	312	91.9	1.9	.7	.6
6			9.7	335	76.2	2.5	1.4	.5
7			9.6	281	77.5	2.0	1.1	.5
8			9.7	631	76.0	2.4	1.1	.9
9	4	168	9.7	404	48.1	4.7	2.1	0.7
10			10.6	418	58.5	4.0	1.8	.6
11			9.7	516	41.0	7.1	2.7	.5
12			9.7	564	63.3	5.0	2.5	.7
13			9.7	370	60.0	3.5	2.1	.9
14			10.6	550	113.0	2.8	2.1	.7
15			9.7	447	49.2	5.1	2.0	1.3
16			9.6	449	56.0	4.6	2.1	1.1
17	4	252	12.3	570	66.0	4.9	2.7	0.9
18			9.9	418	101.4	2.3	2.6	.9
19			10.1	754	65.1	6.5	3.0	.4
20			11.5	703	96.4	4.1	3.3	.6
21			10.0	687	61.4	6.3	3.4	.7
22			10.0	593	67.1	5.0	2.9	.7
23			10.0	465	98.3	2.7	2.1	.7
24			10.6	586	72.2	4.6	3.4	.7
25	4	336	9.7	532	88.2	3.4	2.1	0.8
26			9.7	844	65.3	7.3	3.1	.9
27			9.7	615	80.4	4.3	2.4	.7
28			9.7	959	68.9	7.8	3.0	1.1
29			9.6	638	74.9	4.8	2.9	.7
30			9.6	921	64.9	8.0	3.3	.4
31			11.6	903	66.2	7.6	3.3	.7
32			10.5	624	72.9	4.8	2.9	.6
33	4	420	9.7	705	98.6	4.0	2.8	0.9
34			----	754	117.1	3.6	2.6	.7
35			9.6	835	87.0	5.4	3.0	.5
36			9.7	669	88.6	4.3	2.9	.6
37			9.7	642	89.0	4.1	2.6	1.8
38			10.6	642	89.9	4.0	2.8	.6
39			10.6	683	90.2	4.3	2.8	.7
40			9.6	855	86.4	5.6	2.5	.7
41			9.5	790	83.7	5.3	2.5	.6
42			9.6	656	92.8	4.0	2.4	.9
43	6	210	9.5	1,098	93.5	6.6	4.8	4.6
44			12.5	638	84.6	4.2	4.6	3.7
45			9.5	1,051	87.9	6.7	4.1	2.1
46			9.6	1,033	91.9	6.3	5.0	5.1
47			9.5	837	73.3	6.4	5.6	5.3
48			9.7	990	89.9	6.2	4.9	.9

TABLE II.- Concluded

DATA OBTAINED DURING LANDINGS IN WAVES

[All values are full size; initial landing trim, ≈10°]

(c) l = 8.6 feet

Fixed control

Landing	Wave height, ft	Wave length, ft	τ_L, deg	V_v, ft/min	V, knots	γ, deg	n_v, g units	A, radians/sec^2
1	2	168	9.8	224	68.9	1.8	1.2	0.4
2				220	90.6	1.4	1.4	0
3				144	78.4	1.0	1.2	0
4				238	67.1	2.0	1.2	0
5	4	210	9.7	633	57.8	6.2	2.8	1.1
6			9.8	763	54.3	7.9	2.9	1.3
7			9.8	431	93.5	2.6	2.7	1.3
8			9.8	647	61.4	5.9	3.0	.9
9			9.6	683	94.4	4.1	3.1	1.1
10			9.8	525	63.1	4.7	3.0	.9
11			9.8	530	68.7	4.4	2.9	1.1
12			9.7	768	88.6	4.9	3.4	1.3
13	4	252	9.8	494	89.5	3.1	2.6	0.9
14			9.8	804	52.7	8.6	3.2	1.1
15			9.7	701	89.3	4.4	2.8	.7
16			9.8	624	93.7	3.8	2.7	.9
17			9.7	799	91.9	4.9	3.1	1.8
18			9.7	804	93.3	4.9	3.1	1.8
19			9.8	537	67.3	4.5	2.7	.9
20			9.7	772	98.3	4.4	3.2	1.1
21	4	336	9.8	851	105.9	4.5	2.9	1.1
22			9.8	714	84.8	4.7	2.9	.6
23			9.8	790	71.5	6.2	2.7	.6
24			9.8	665	82.2	4.6	3.0	.4
25			9.7	768	62.7	6.9	3.0	.7
26			9.7	633	85.1	4.2	2.9	.7
27			9.8	804	73.5	6.2	2.4	.7
28			9.7	714	85.9	4.7	2.7	.6
29	4	420	9.8	739	77.5	5.4	2.7	0.9
30			9.7	656	87.0	4.2	2.4	.7
31			9.7	802	85.1	5.3	2.6	1.1
32			9.7	822	80.8	5.7	2.6	.7
33			9.8	680	82.0	4.7	2.6	.9
34			9.7	678	88.4	4.3	2.5	.7
35			9.8	759	67.8	6.3	2.0	.9
36			9.7	698	89.7	4.4	2.4	.7

With aerodynamic pitch damping

Landing	Wave height, ft	Wave length, ft	τ_L, deg	V_v, ft/min	V, knots	γ, deg	n_v, g units	A, radians/sec^2
37	4	168	9.8	132	87.7	0.8	1.2	0.7
38			9.9	496	49.8	5.1	2.6	1.4
39			9.8	397	57.6	3.9	2.4	.7
40			9.8	629	41.6	8.5	3.0	1.1
41			9.8	445	50.7	4.9	2.3	.7
42			9.8	546	44.5	6.9	2.8	.9
43			9.8	489	47.0	5.9	2.3	.7
44			9.8	427	55.4	4.4	2.0	.7
45	4	252	8.9	568	80.0	4.0	3.0	0.9
46			9.6	566	68.2	4.7	2.8	.9
47			9.6	727	108.5	3.8	3.0	.7
48			9.8	629	68.4	5.2	2.8	.7
49			9.8	712	69.3	5.8	2.7	.7
50			9.7	674	60.7	6.2	2.9	.7
51			9.7	487	65.9	2.9	2.6	.7
52			9.9	694	70.2	5.6	2.5	.9
53	4	336	9.8	689	74.0	5.2	3.0	0.7
54				983	70.9	7.8	2.9	0
55				638	66.9	5.4	2.7	0
56				736	66.2	6.3	2.6	.9
57				853	71.8	6.7	2.8	.6
58				570	76.9	4.2	2.7	.9
59				777	74.6	5.9	2.5	.5
60				804	67.1	6.7	2.7	.9

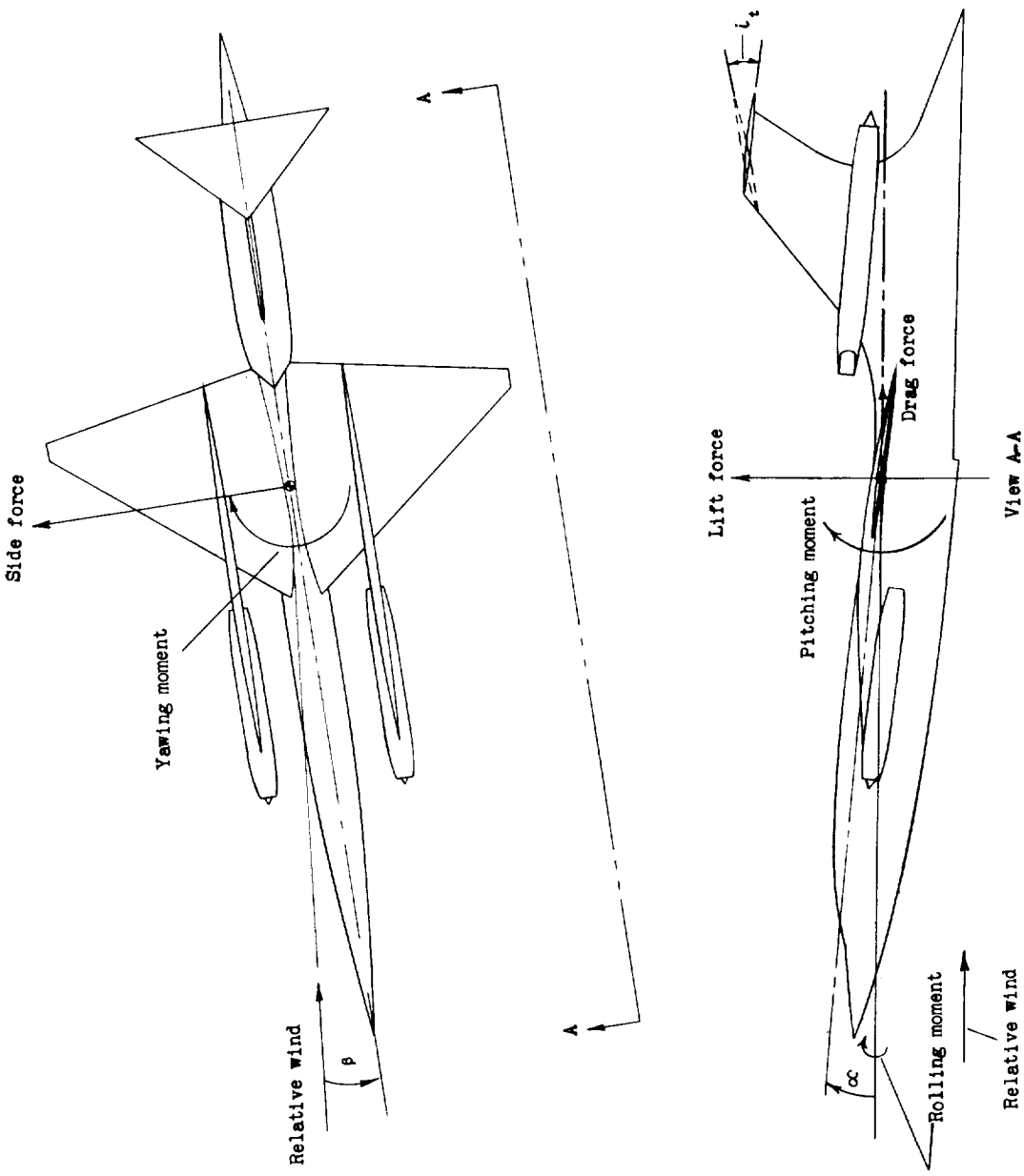

Figure 1.- Stability-axes system.

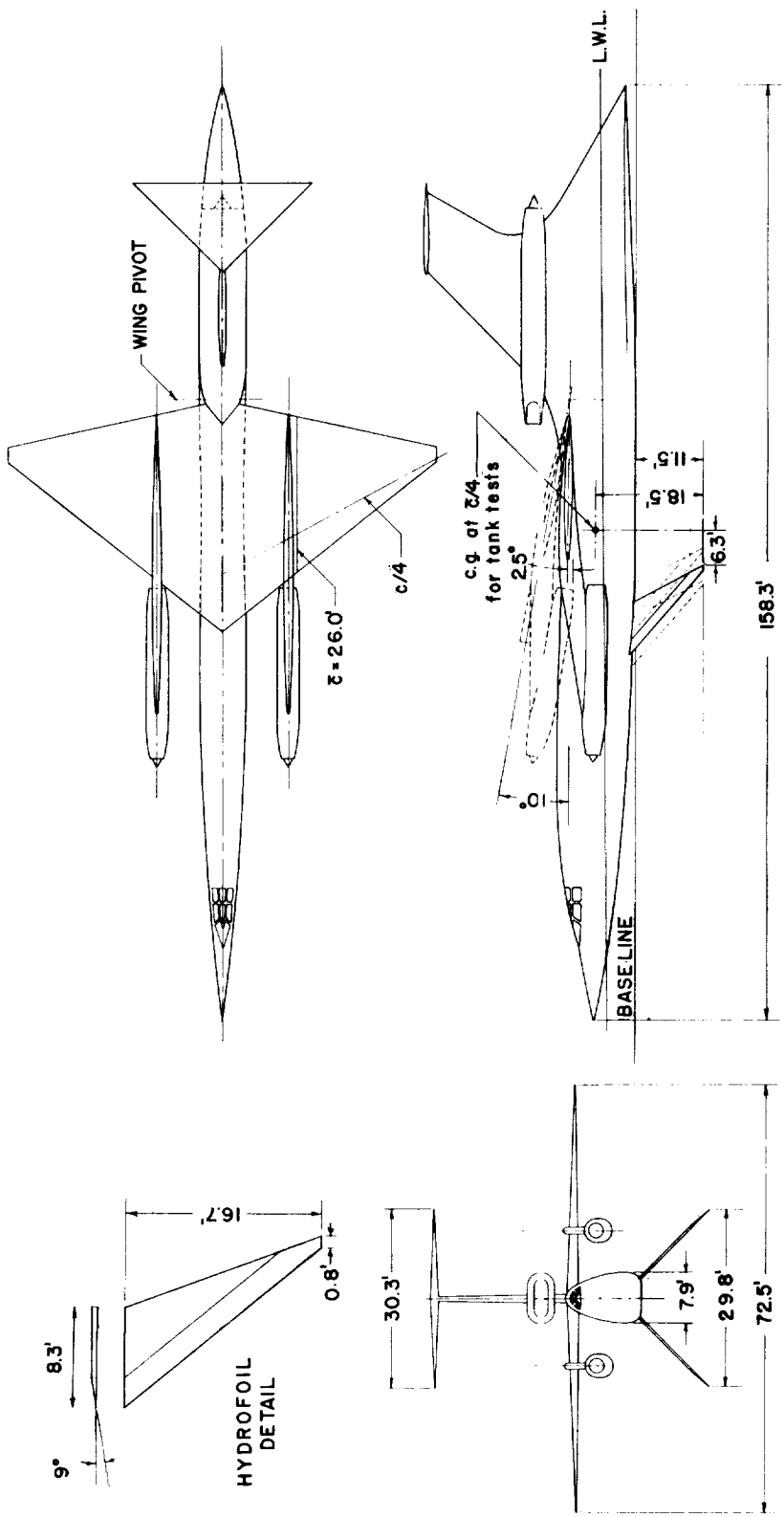

Figure 2.- General arrangement of configuration with hydrofoil gear. Dimensions are full size.

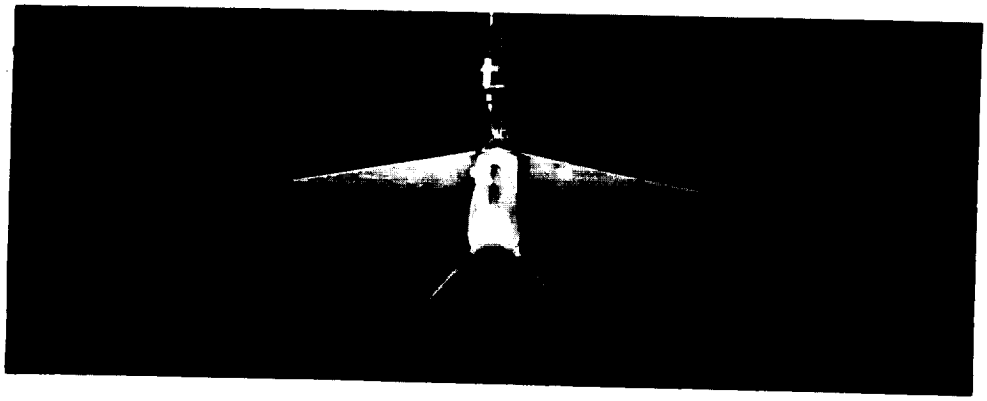

(a) Front view. L-58-1495

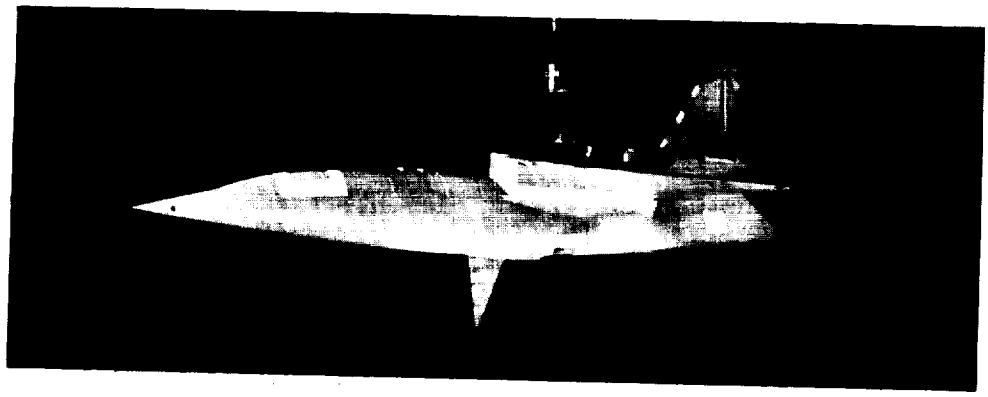

(b) Three-quarter front view. L-58-1496

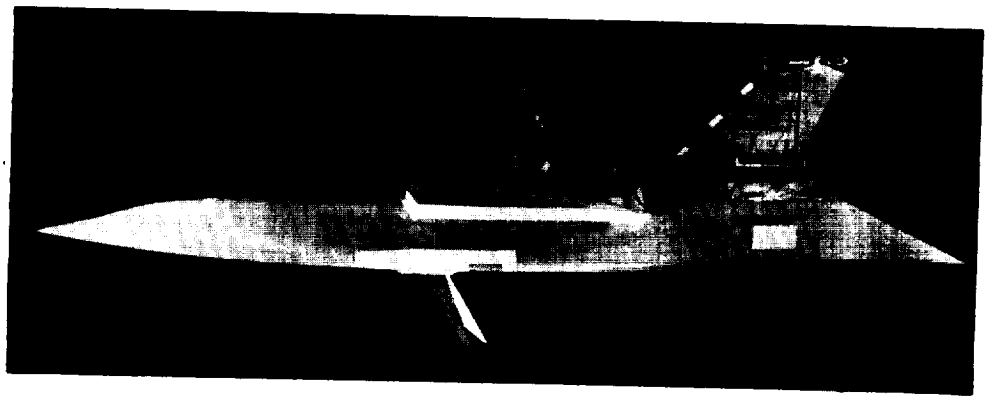

(c) Side view. L-58-1498

Figure 3.- The 1/14-scale dynamic model of the hydrofoil configuration

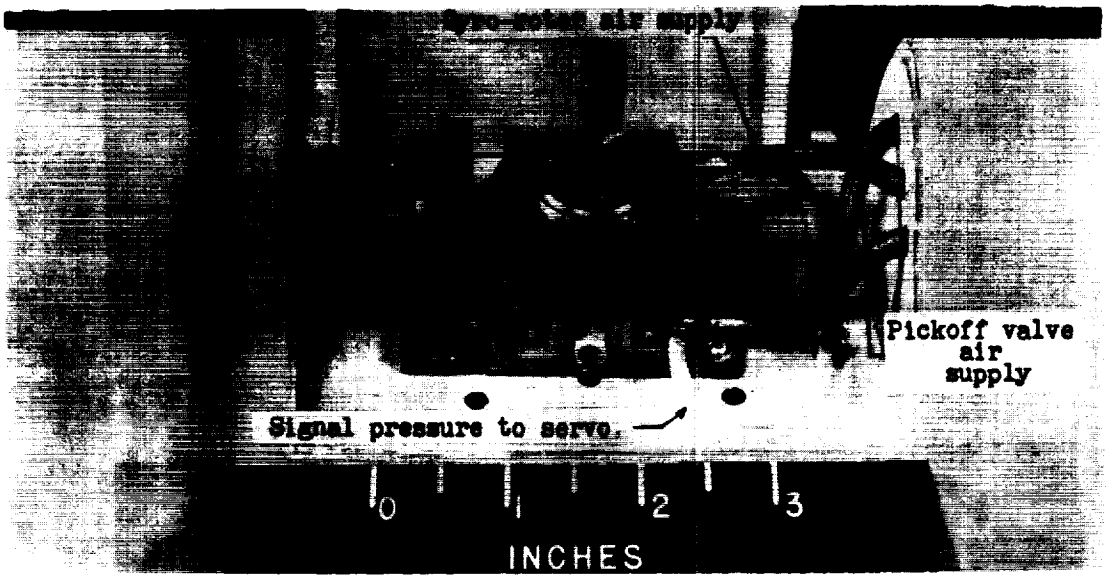

(a) Rate-gyro sensing element. L-57-5536.1

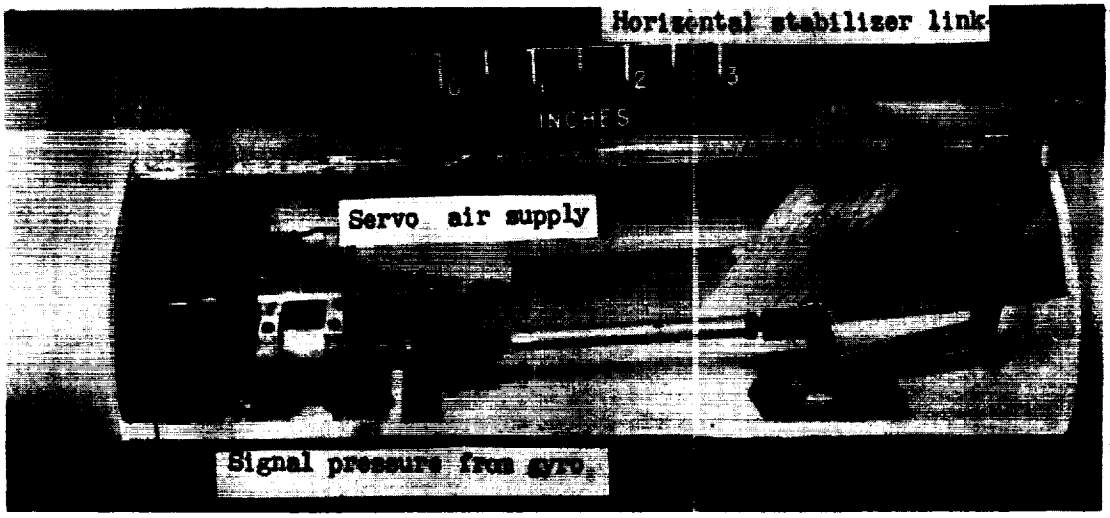

(b) Pneumatic servoactuator and tail linkage. L-58-437.1

Figure 4.- Artificial-stabilization system for providing aerodynamic pitch damping.

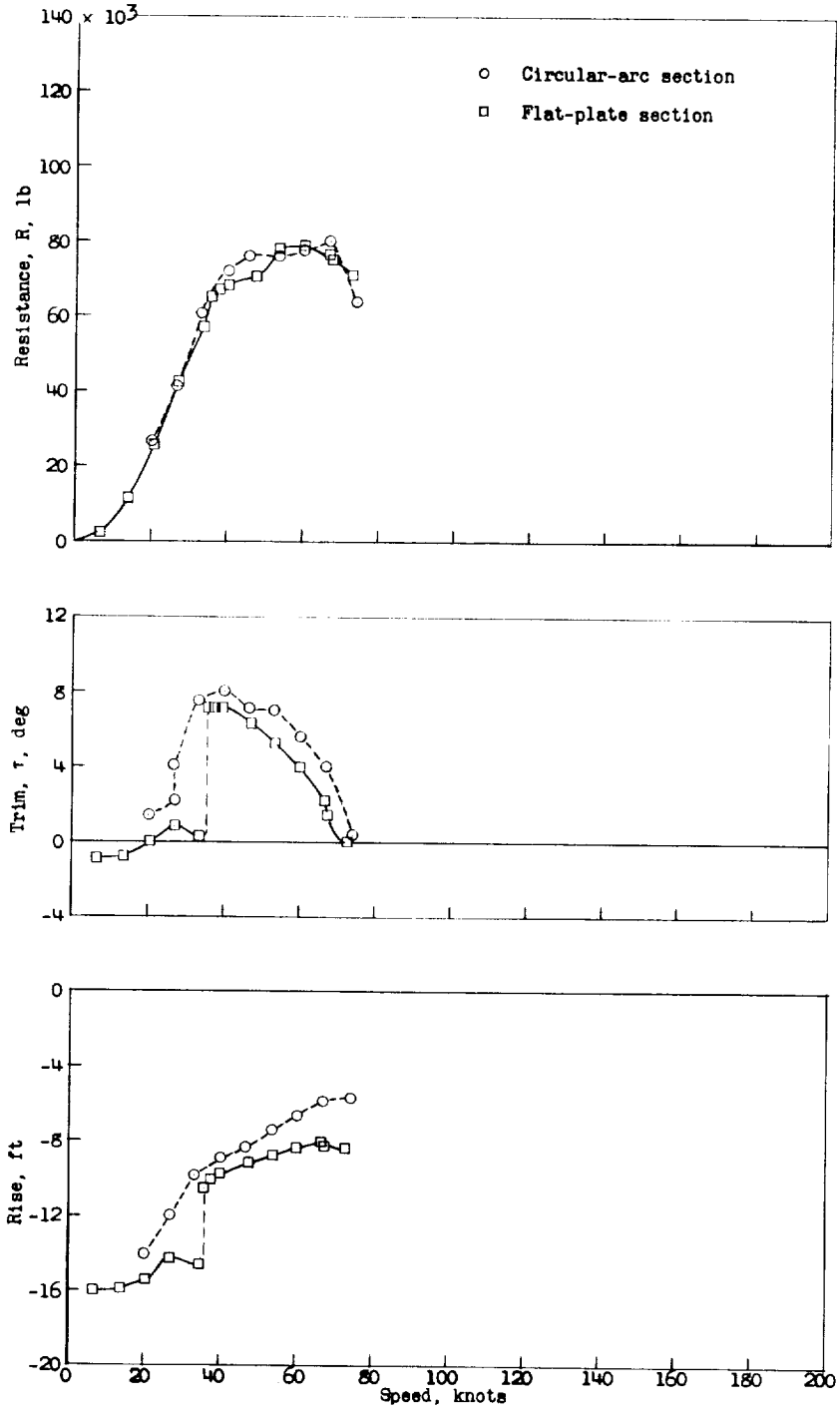

Figure 5.- Variation of free-to-trim total resistance, trim, and rise of the center of gravity with speed in smooth water. Δ_o = 197,000 pounds.

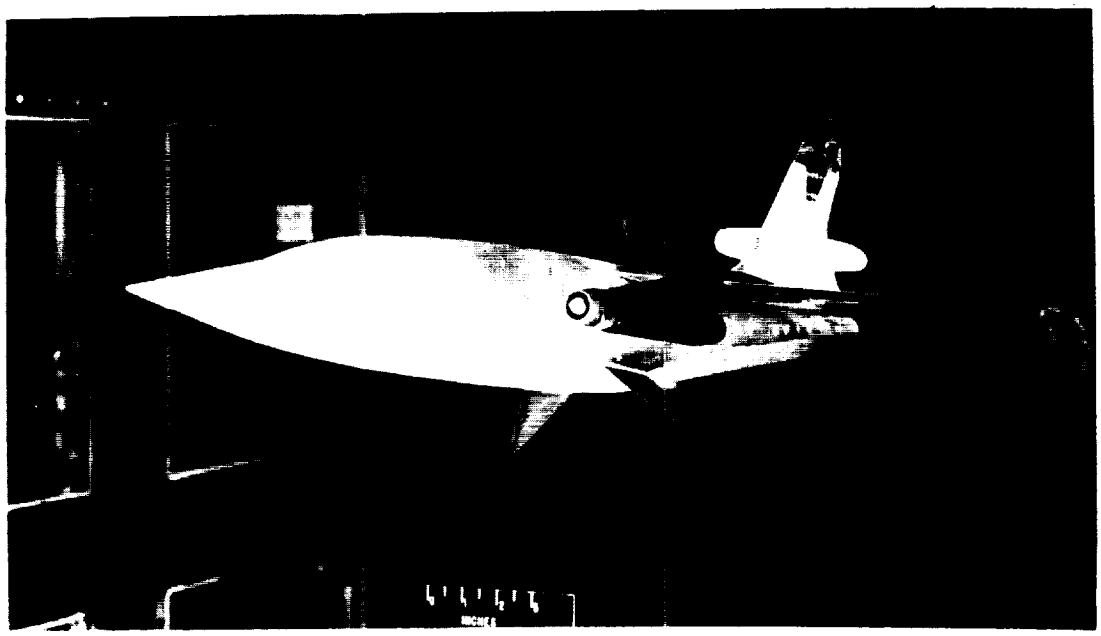

L-57-4014

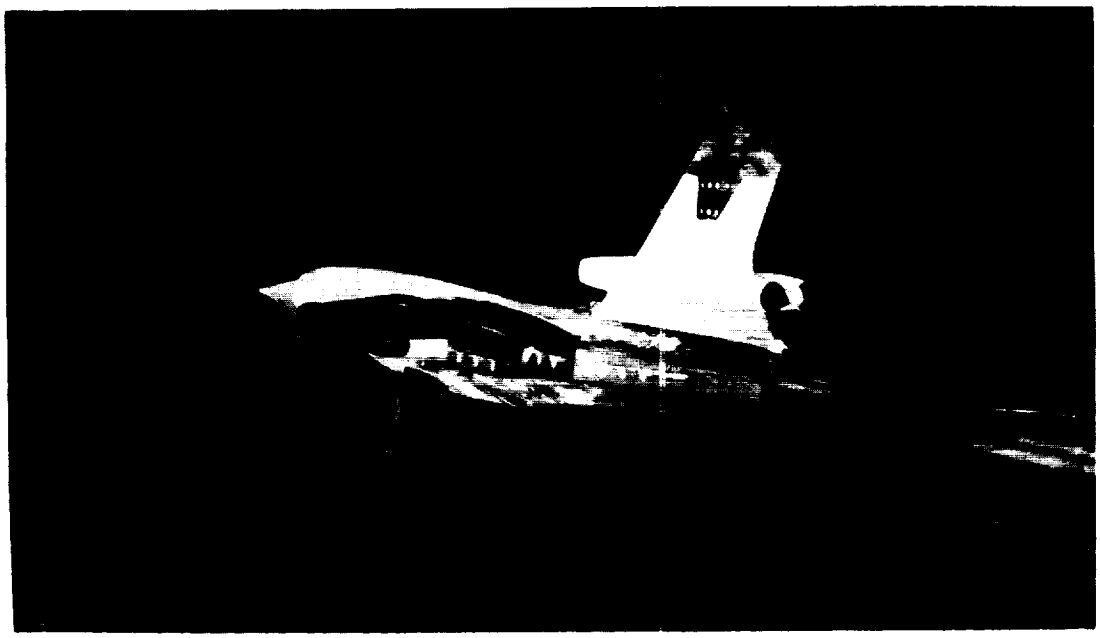

L-57-4015

Figure 6.- Sting-mounted 1/42.5-size hull model with hydrofoils in the Langley 8-foot transonic pressure tunnel.

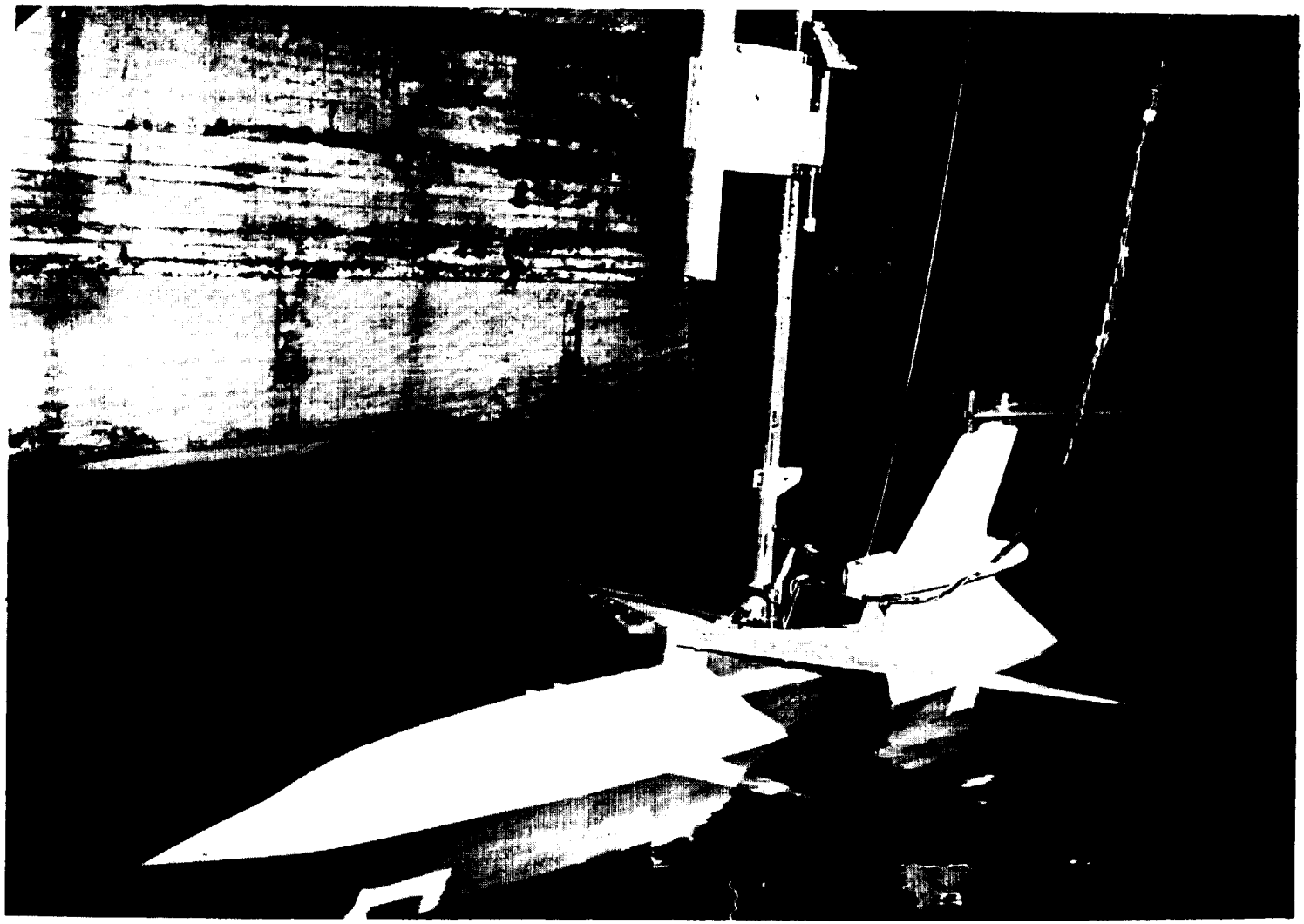

Figure 7.- Model on tank towing gear. L-58-2759

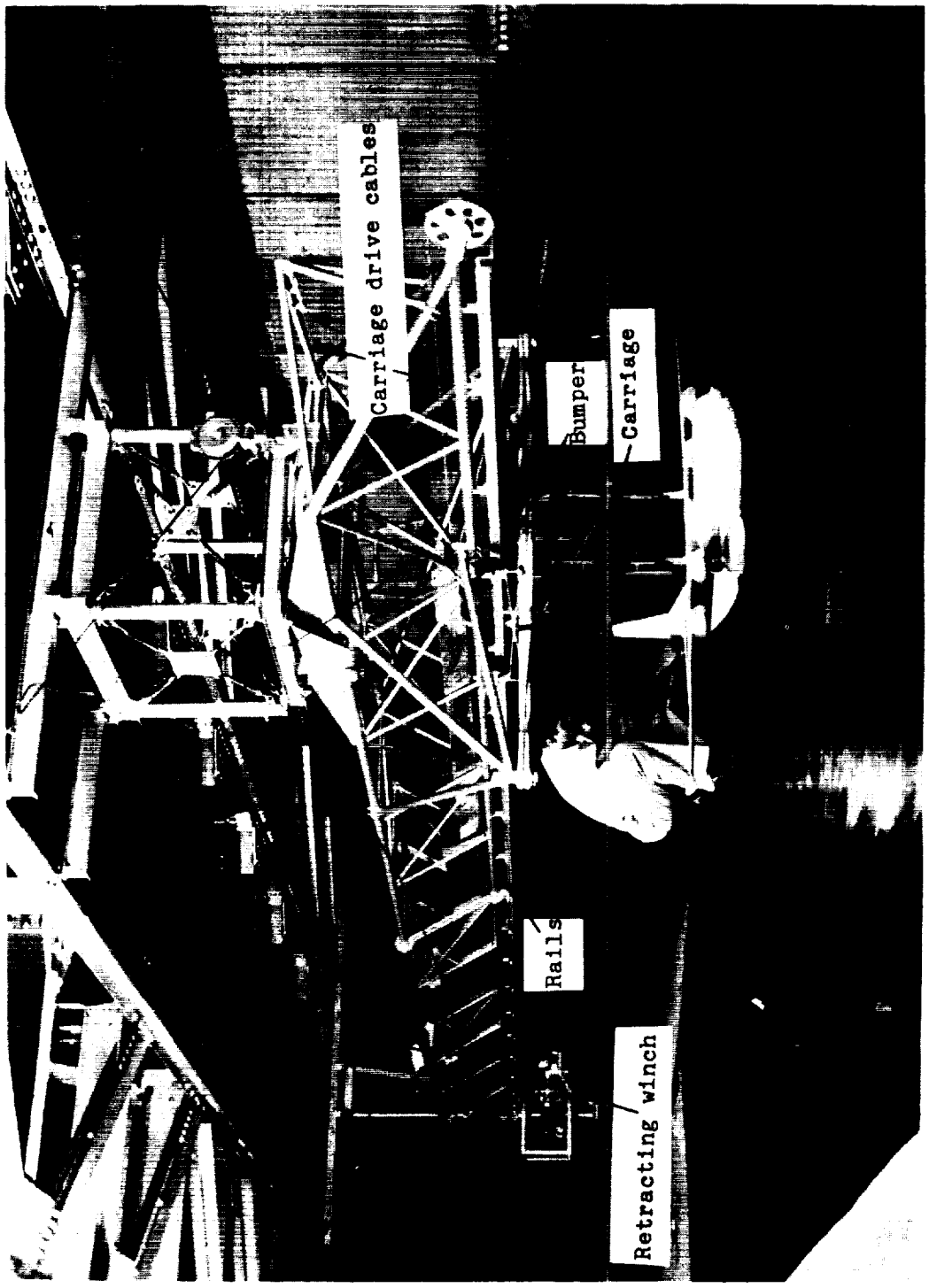

Figure 8.- Photograph of catapult. L-94761.1

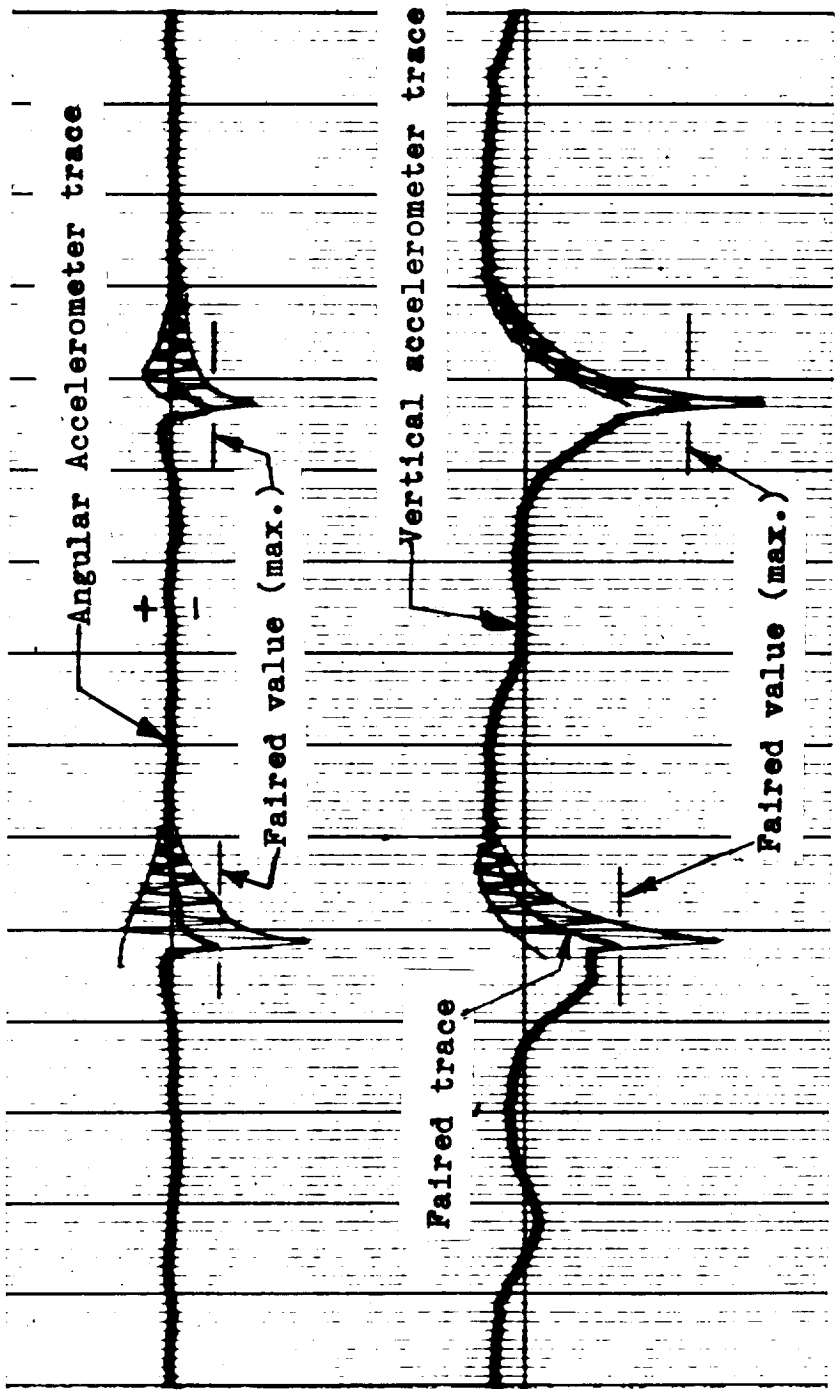

Figure 9.- Typical oscillograph accelerometer traces showing application of the "envelope method" of fairing the impact-loads data.

V= 23.3 knots; $\tau = 0.7^{\circ}$; $\sigma_s = -10^{\circ}$

V= 44.8 knots; $\tau = 6.2^{\circ}$; $\sigma_s = -10^{\circ}$

V= 67.4 knots; $\tau = 5.5^{\circ}$; $\sigma_s = -10^{\circ}$

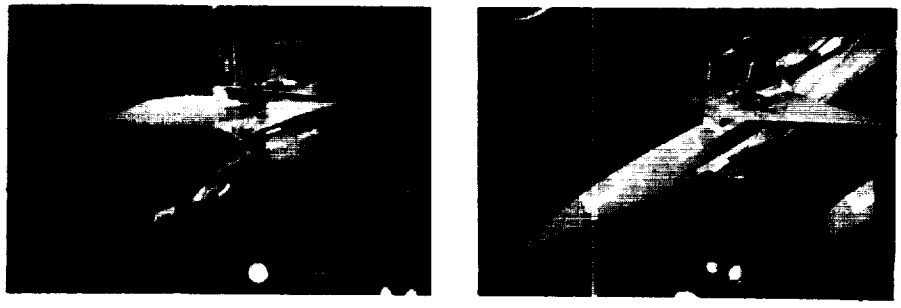

V= 90.8 knots; $\tau = 3.2^{\circ}$; $\sigma_s = -10^{\circ}$

L-59-6064

Figure 10.- Smooth-water-spray photographs of model during constant-speed runs. Δ_0 = 225,000 pounds.

V= 112.5 knots; $\tau = 6.4^{\circ}$; $\alpha_s = -10^{\circ}$

V= 123.2 knots; $\tau = 7.1^{\circ}$; $\alpha_s = -10^{\circ}$

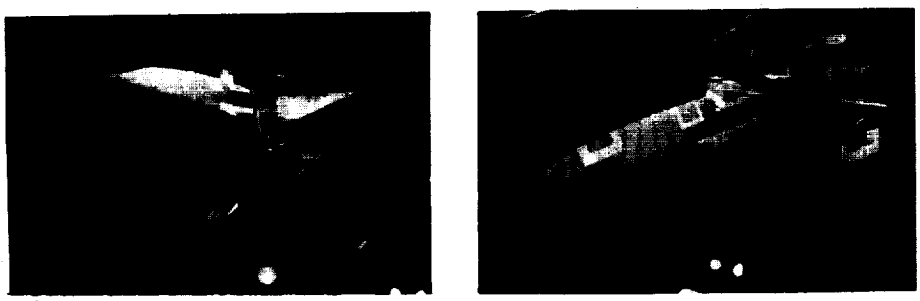

V= 157.0 knots; $\tau = 9.1^{\circ}$; $\alpha_s = -10^{\circ}$

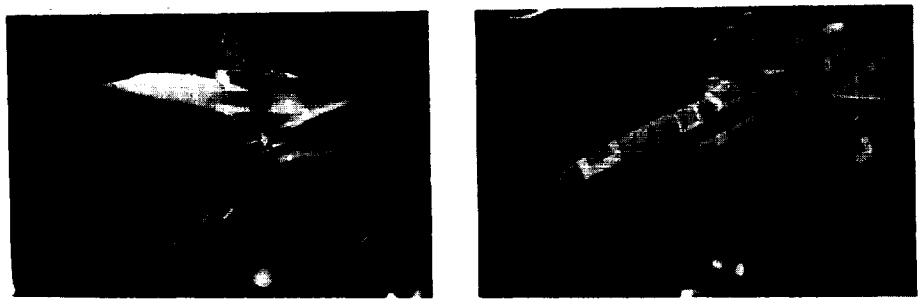

V= 179.7 knots; $\tau = 6.5^{\circ}$; $\alpha_s = -5^{\circ}$

Figure 10.- Concluded. L-59-6065

L-59-6066

Figure 11.- Spray photograph showing concentrated inboard wake blister generated by a pair of negative-dihedral hydrofoils.

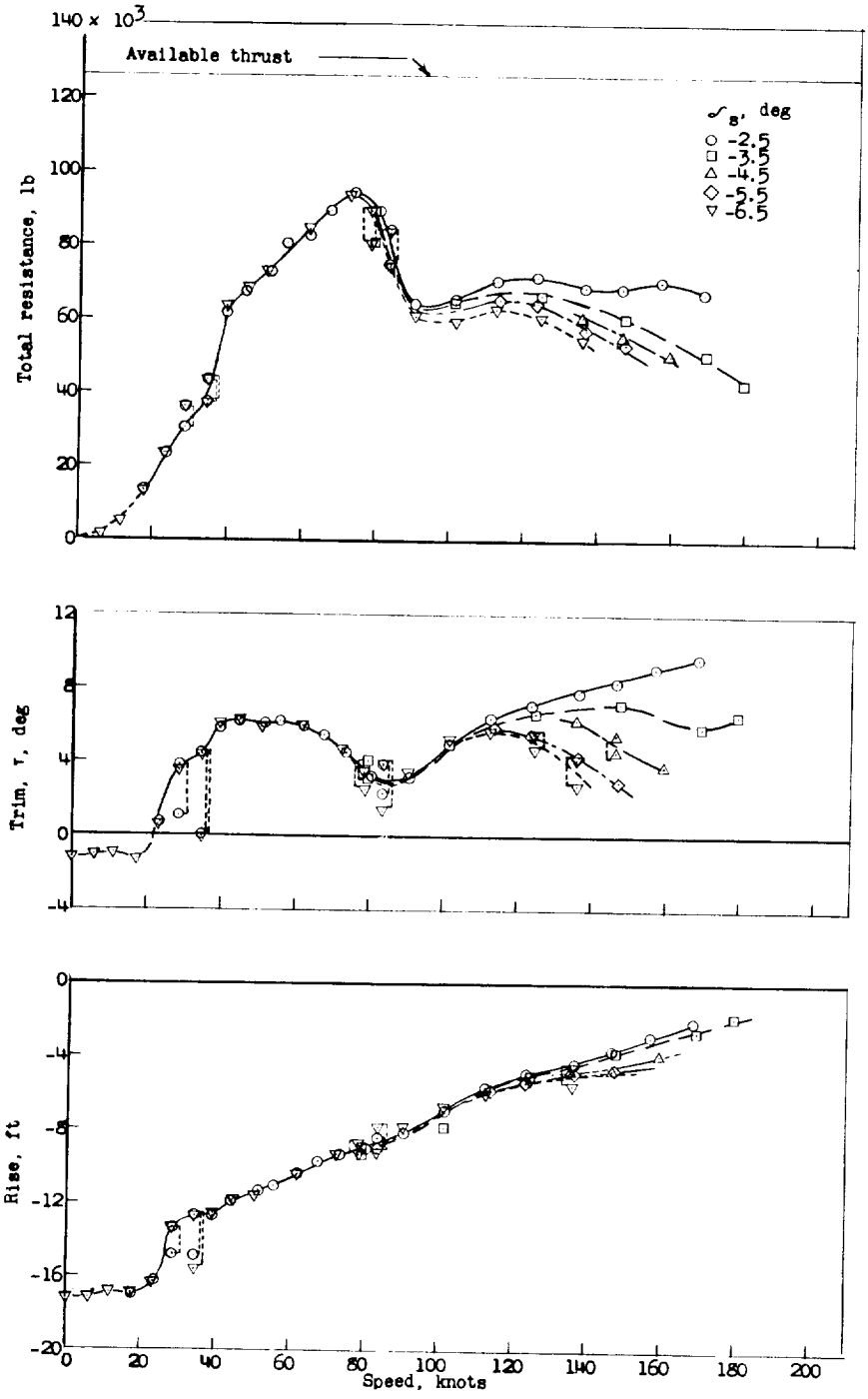

Figure 12.- Variation of free-to-trim total resistance, trim, and rise with speed in smooth water. Δ_o = 225,000 pounds; l = 6.3 feet; fixed stabilizer.

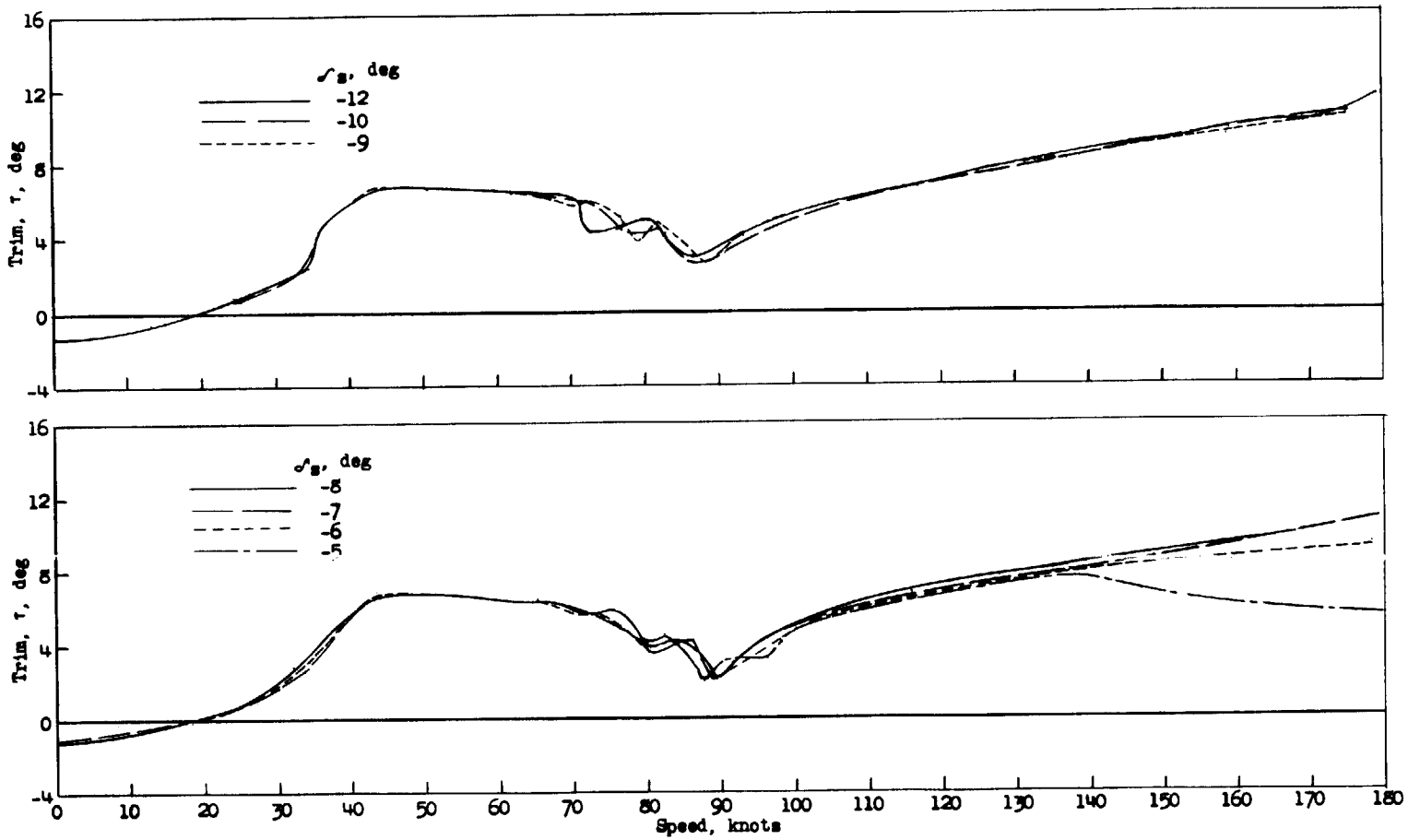

Figure 13.- Variation of trim with speed during takeoff in smooth water. Δ_0 = 225,000 pounds; l = 6.3 feet.

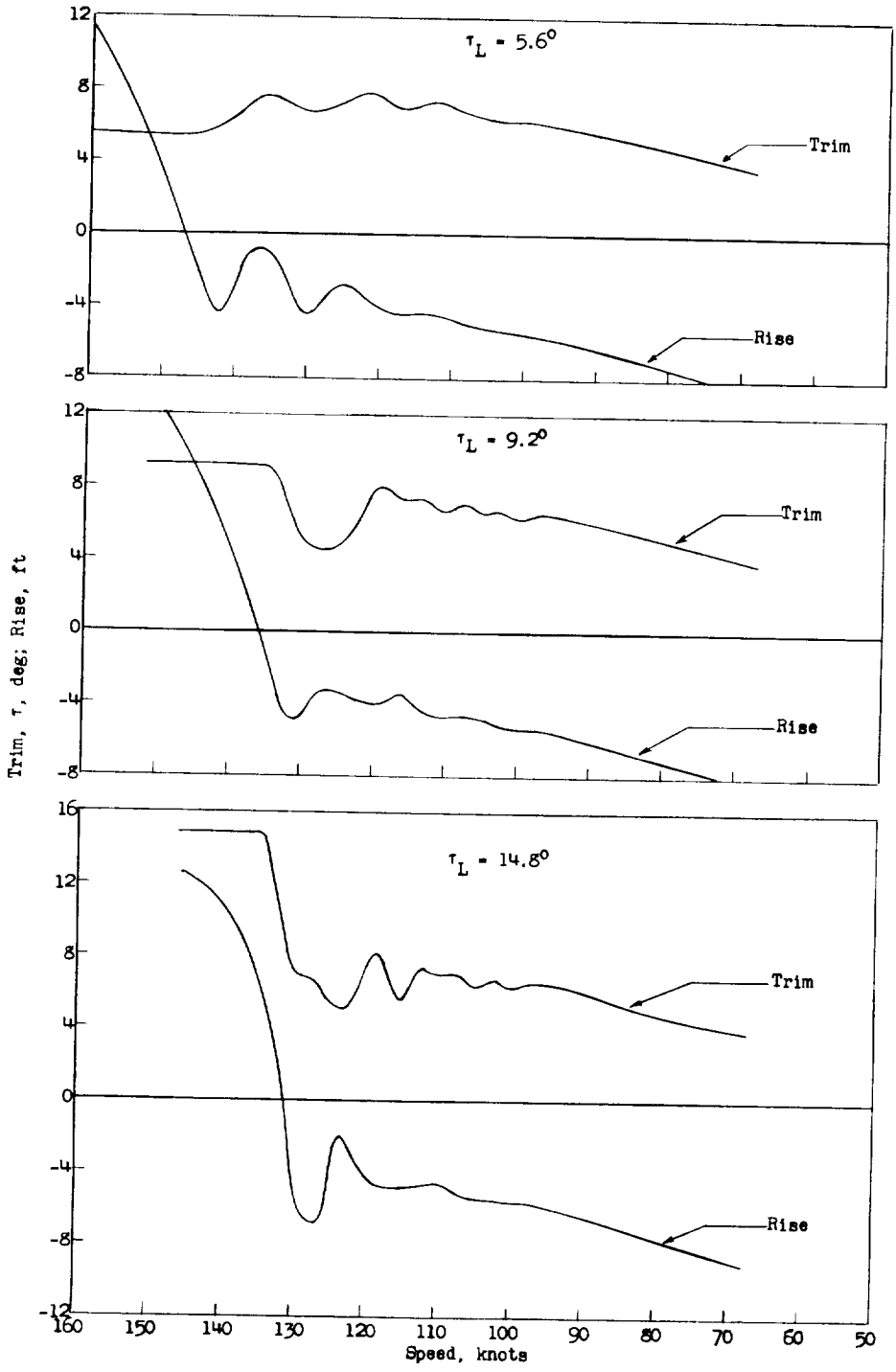

Figure 14.- Variation of trim and rise with speed during smooth-water landings. Δ_0 = 150,000 pounds; l = 6.3 feet.

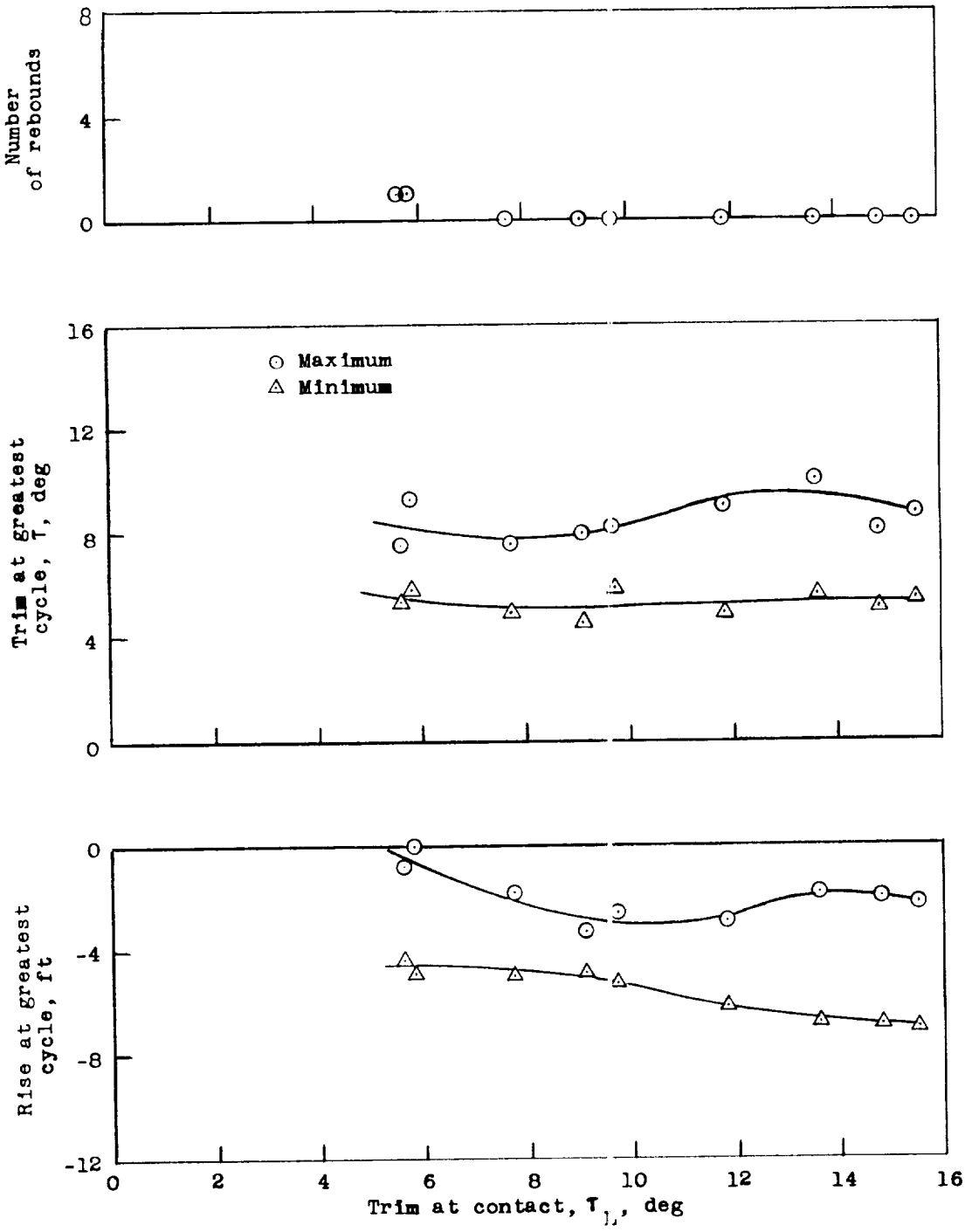

Figure 15.- Maximum variation in trim and rise and the number of rebounds during smooth-water landings. Δ_0 = 150,000 pounds; l = 6.3 feet.

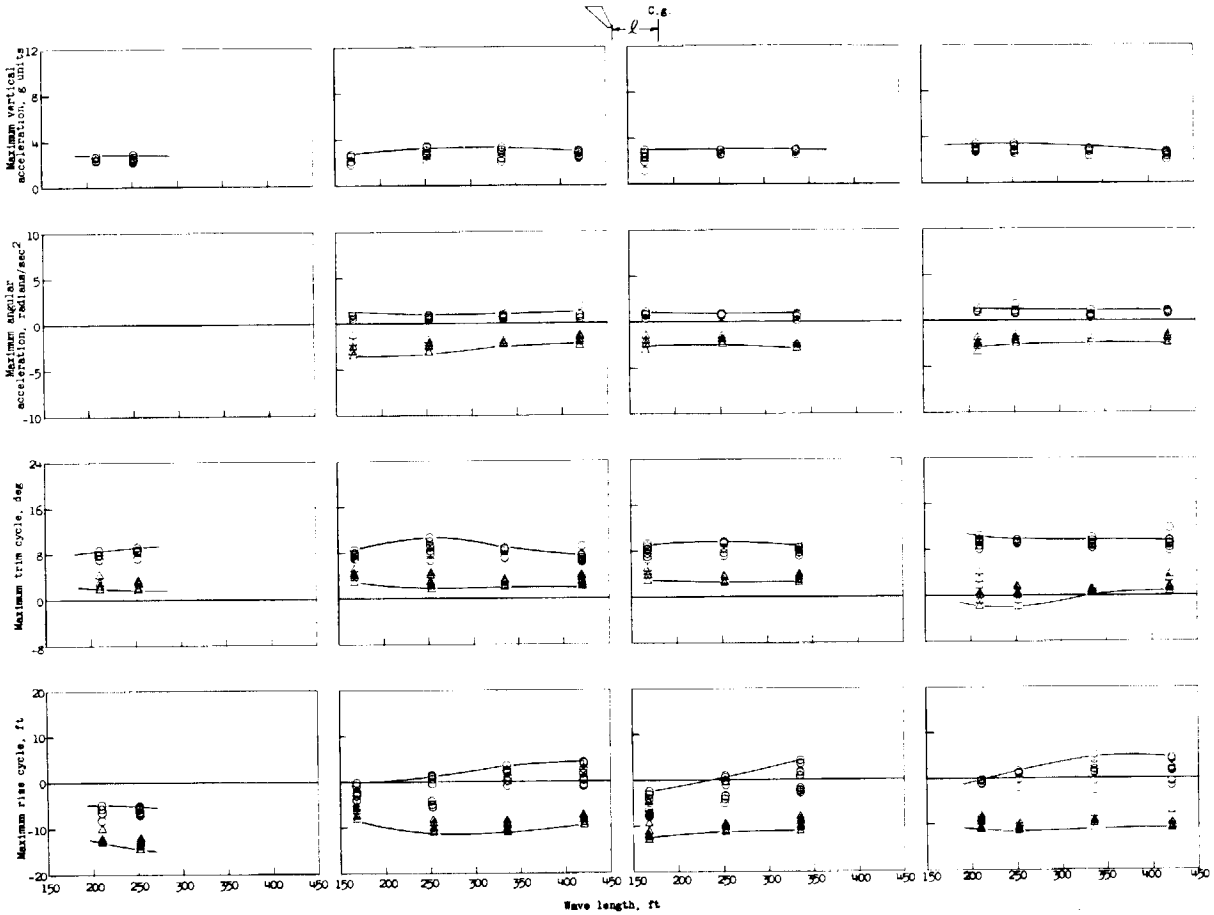

(a) With pitch damping. ℓ = 3.0 feet.
(b) With pitch damping. ℓ = 6.3 feet.
(c) With pitch damping. ℓ = 8.6 feet.
(d) Fixed control. ℓ = 8.6 feet.

Figure 16.- Variation of maximum vertical acceleration, maximum positive and negative angular acceleration, and maximum trim and rise cycle with wave length. Wave height, 4 feet; Δ_o = 150,000 pounds.

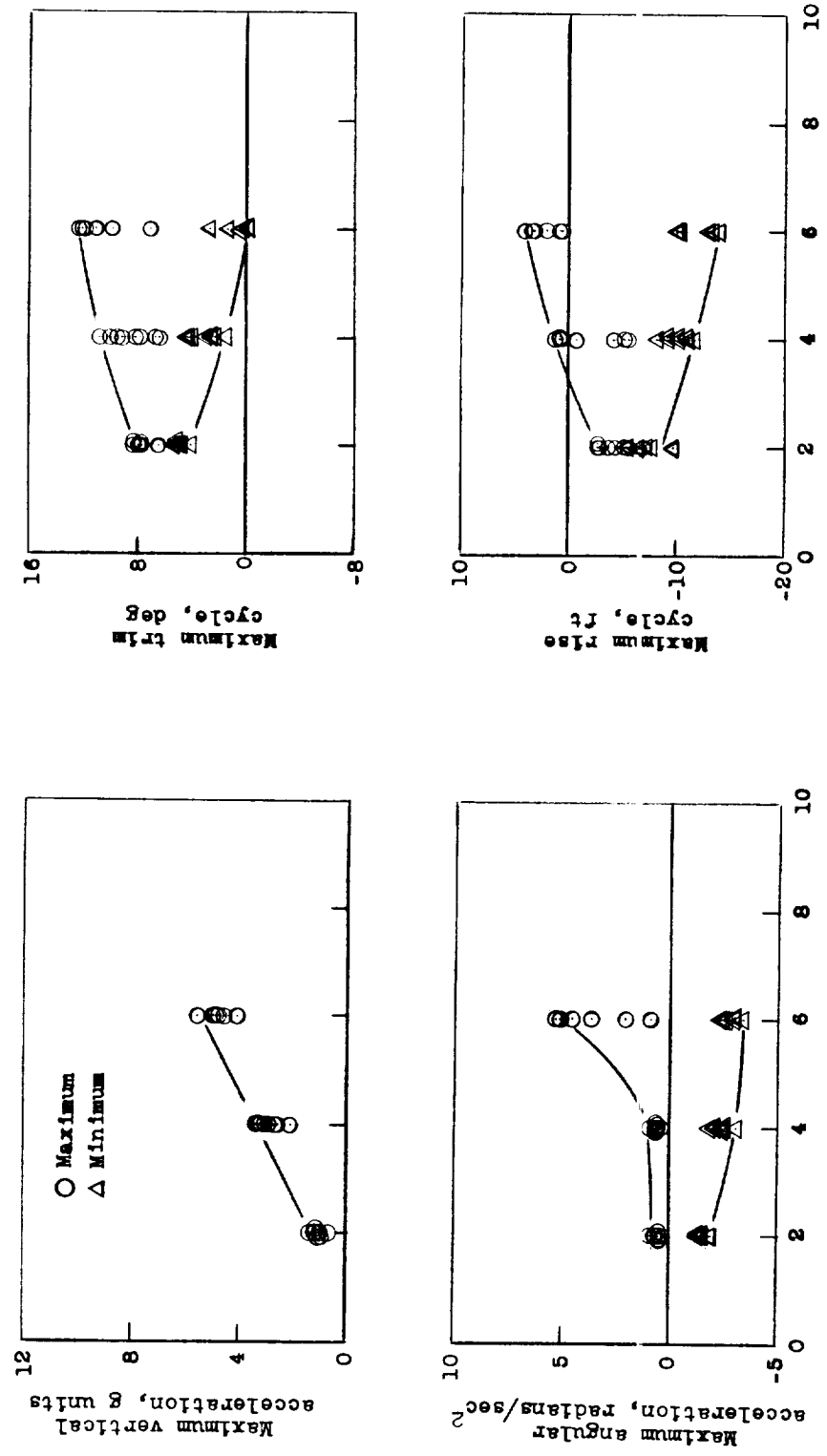

Figure 17.- Effect of wave height on rough-water landing characteristics. Hydrofoil position 1, 6.3 feet; with added aerodynamic pitch damping.

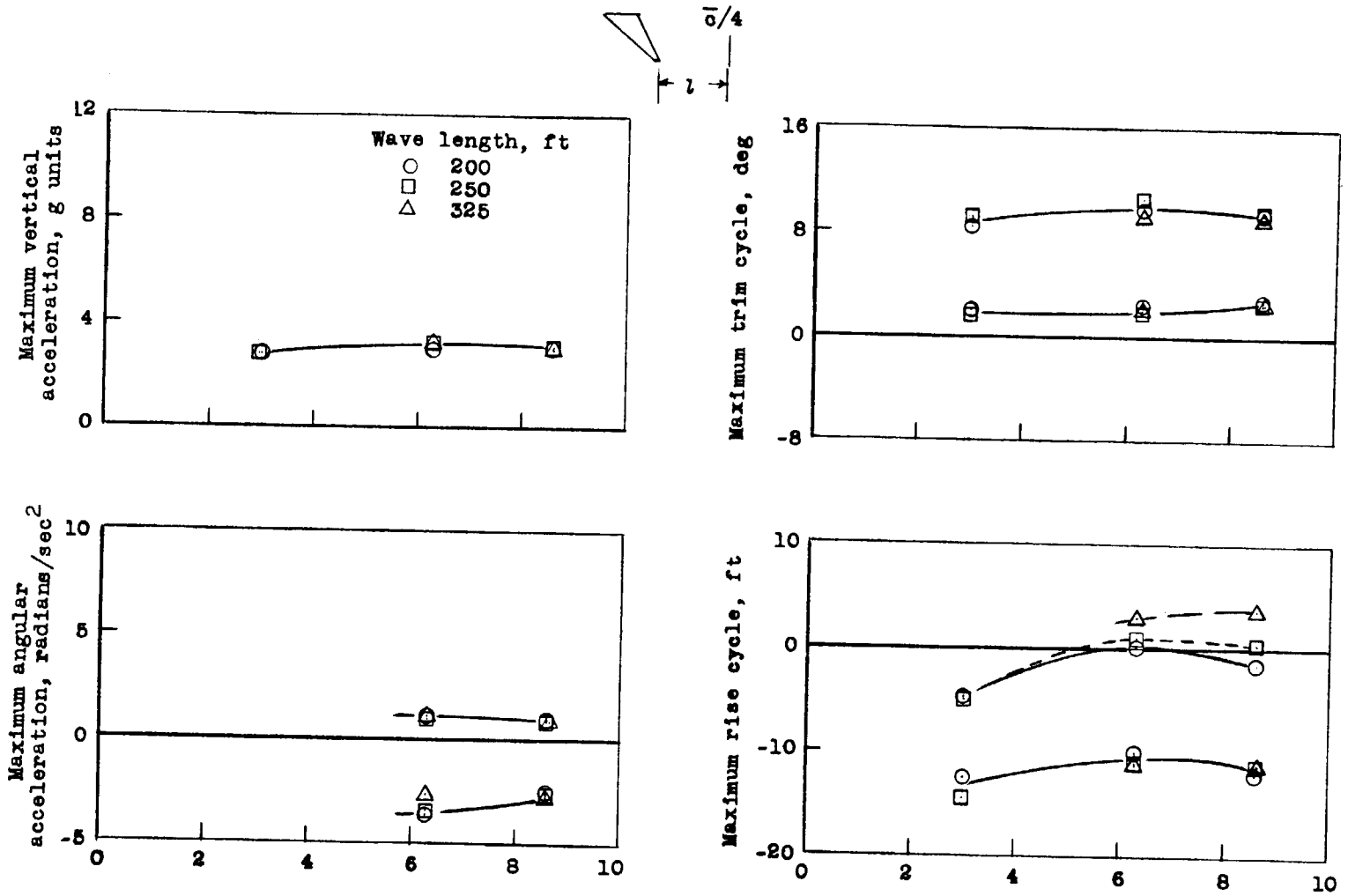

Figure 18.- Effect of hydrofoil longitudinal position l on rough-water landing characteristics for several wave lengths. Wave height, 4 feet; with added aerodynamic pitch damping.

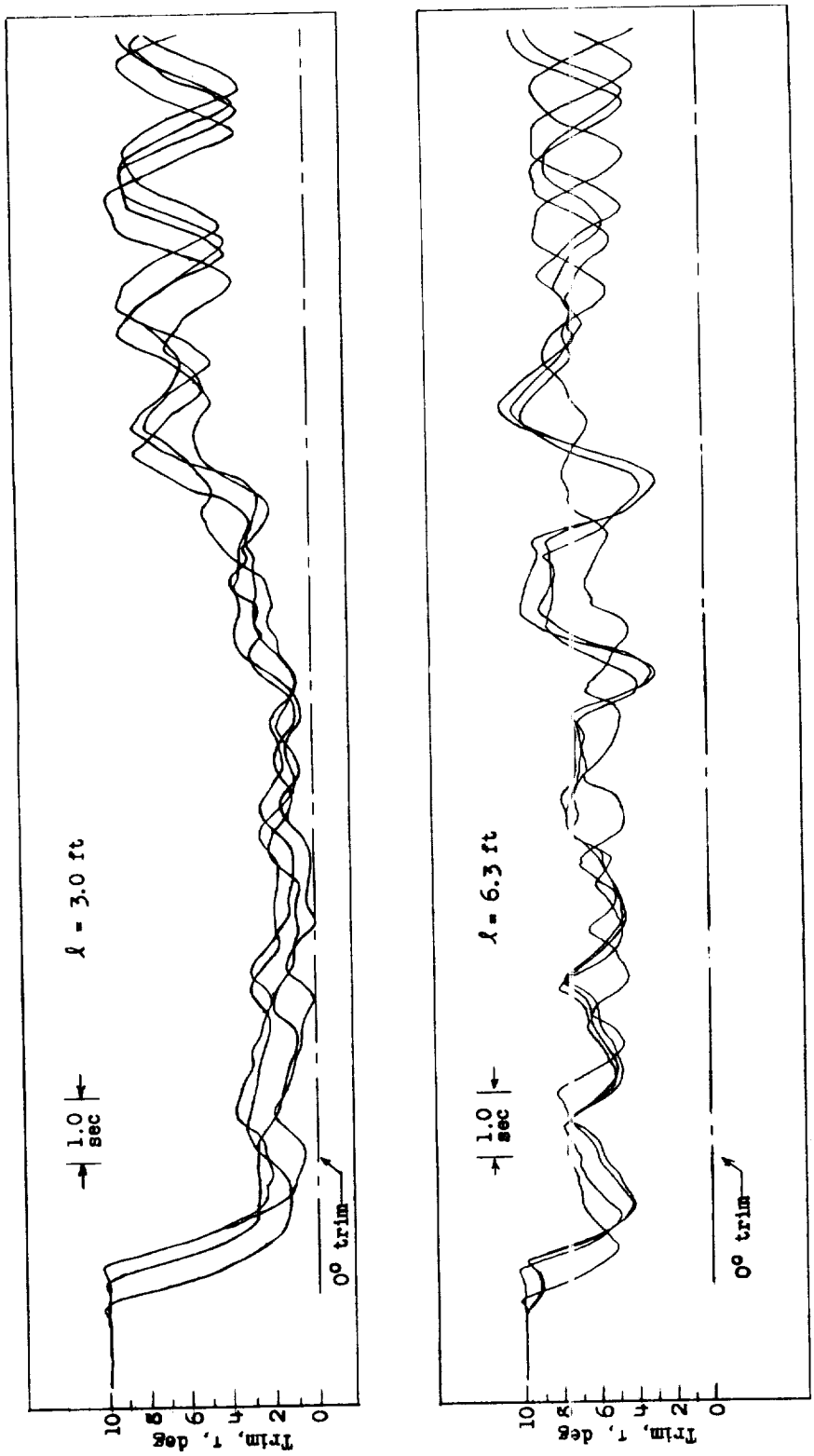

Figure 19.- Effect of hydrofoil longitudinal position l on pitching motions during rough-water landings. Wave height, 4 feet; wave length, 252 feet; with added aerodynamic pitch damping.

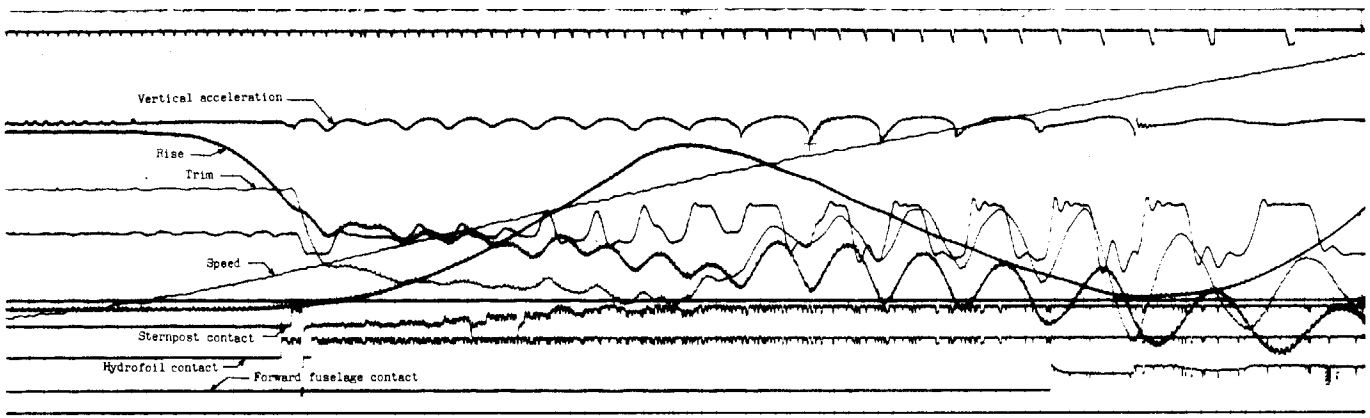

(a) l = 3.0 feet.

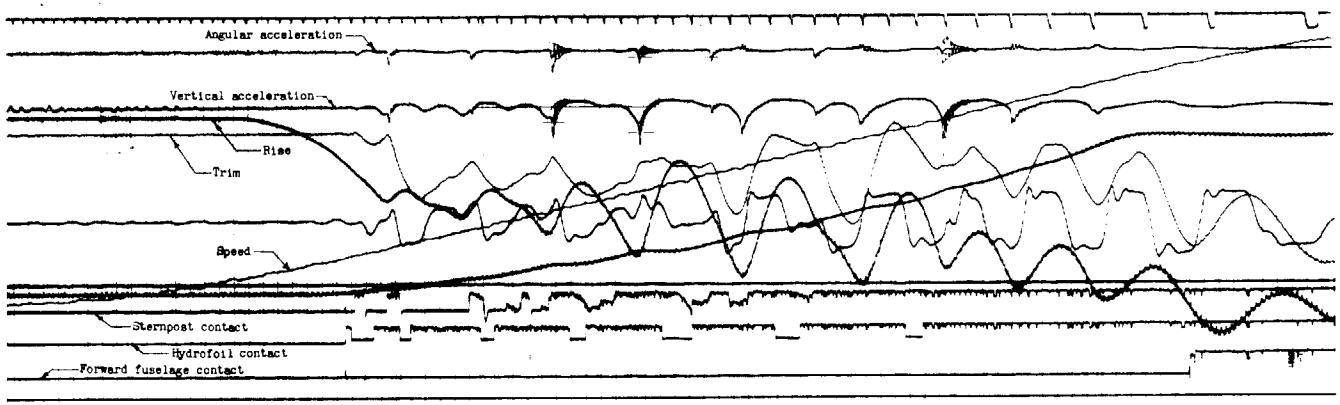

(b) l = 6.3 feet.

Figure 20.- Typical records of a landing in waves for two hydrofoil positions. Wave height, 4 feet; wave length, 252 feet.

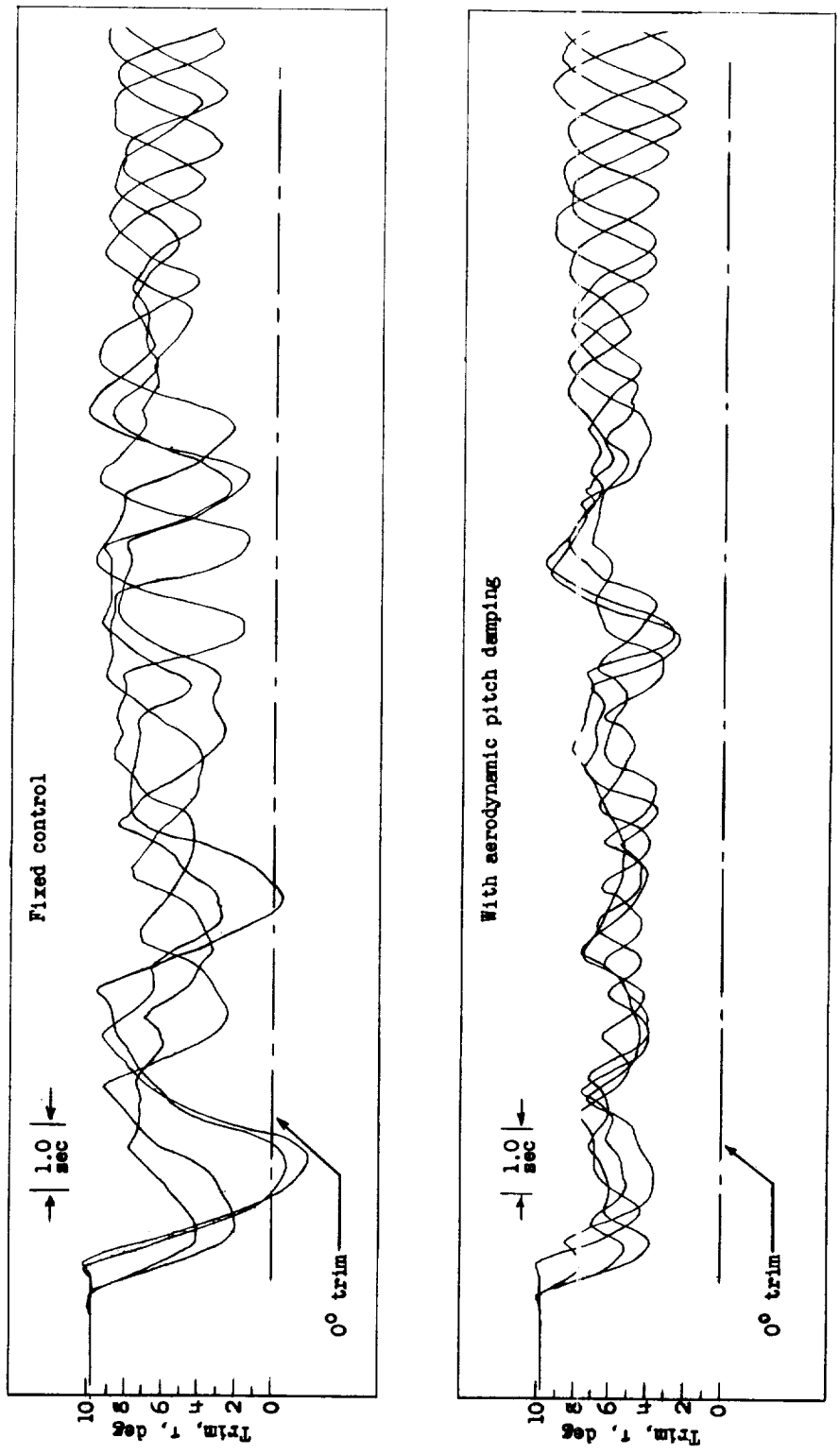

Figure 21.- Effect of added aerodynamic pitch damping on pitching motions during rough-water landings. Wave height, 4 feet; hydrofoil position l, 8.6 feet.

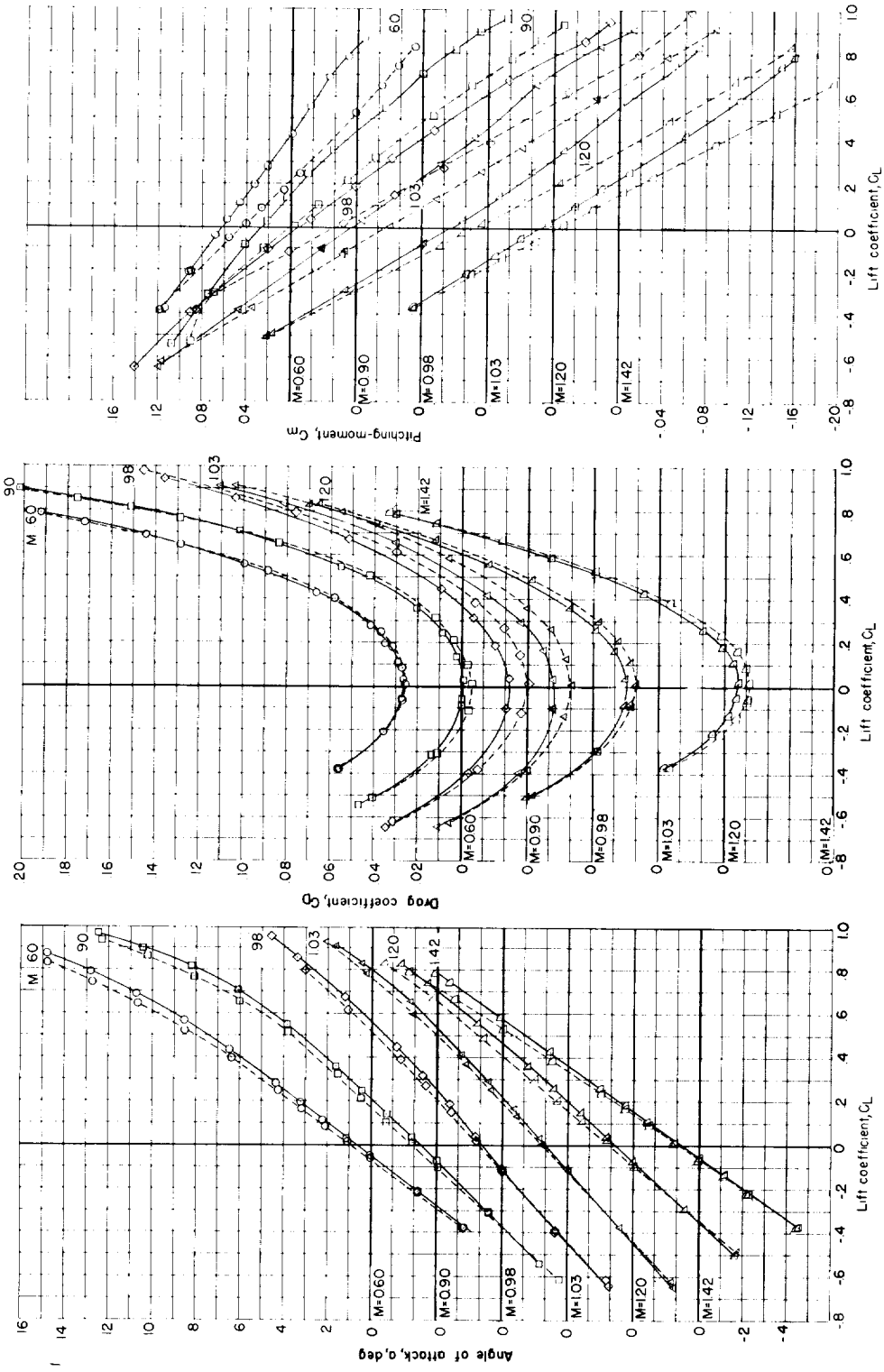

Figure 22.- Aerodynamic characteristics of hull model with and without hydrofoils. Natural transition; $i_t = -2.5°$; stagnation pressure, 0.5 atmosphere.

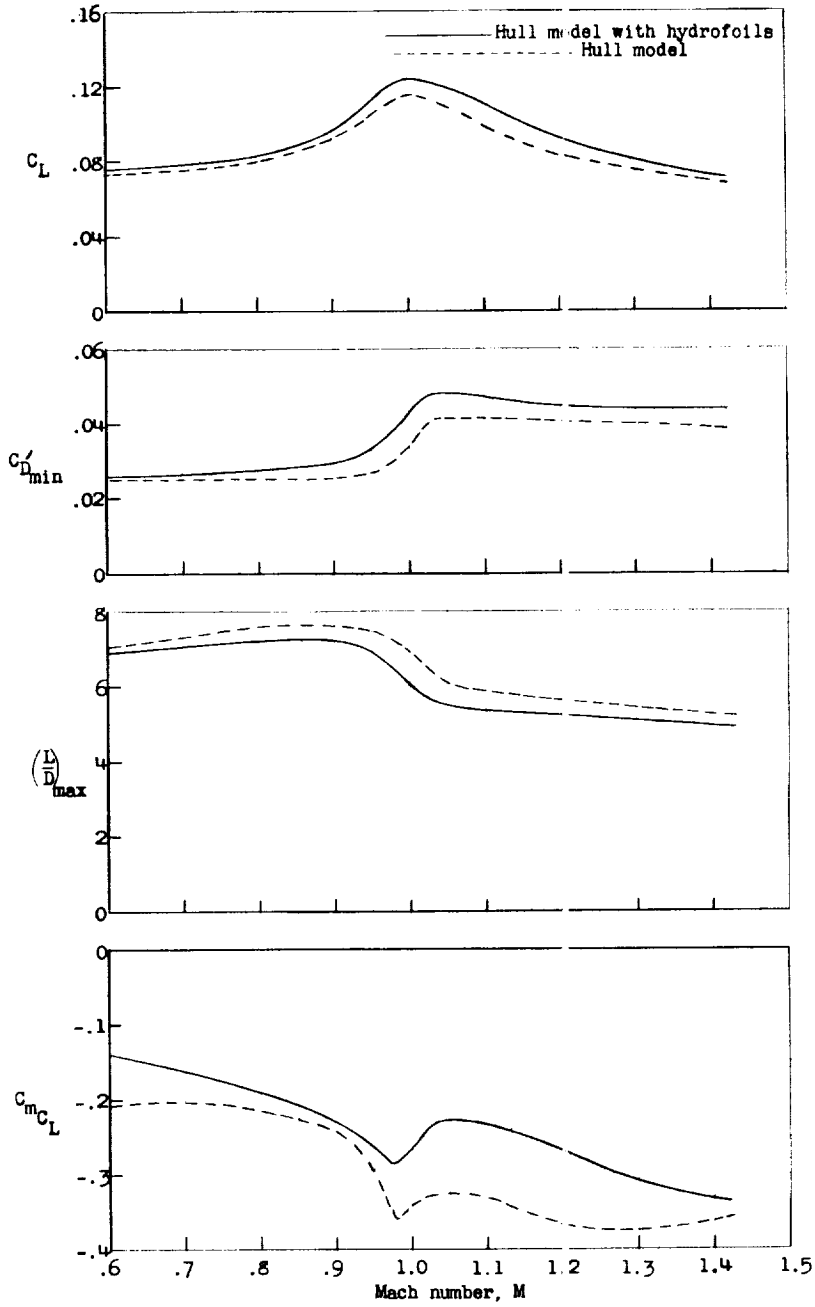

Figure 23.- Summary of static longitudinal aerodynamic characteristics of hull model with and without hydrofoils over the transonic speed range. Natural transition; $i_t = -2.5^\circ$; stagnation pressure, 0.5 atmosphere.

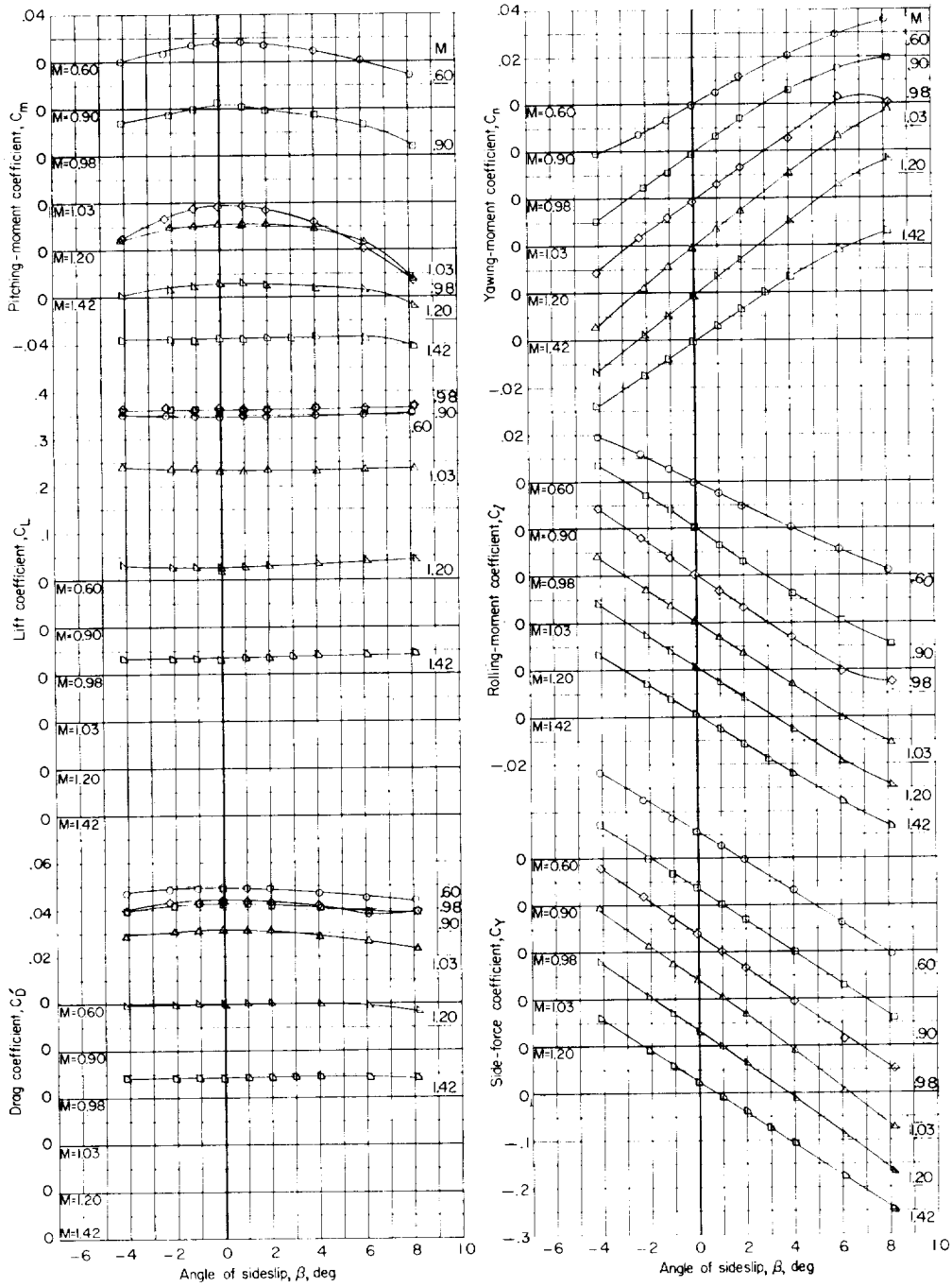

Figure 24.- Aerodynamic characteristics in sideslip of hull model with hydrofoils. Natural transition; $i_t = -2.5^\circ$; stagnation pressure, 0.5 atmosphere; $\alpha \approx 5^\circ$.

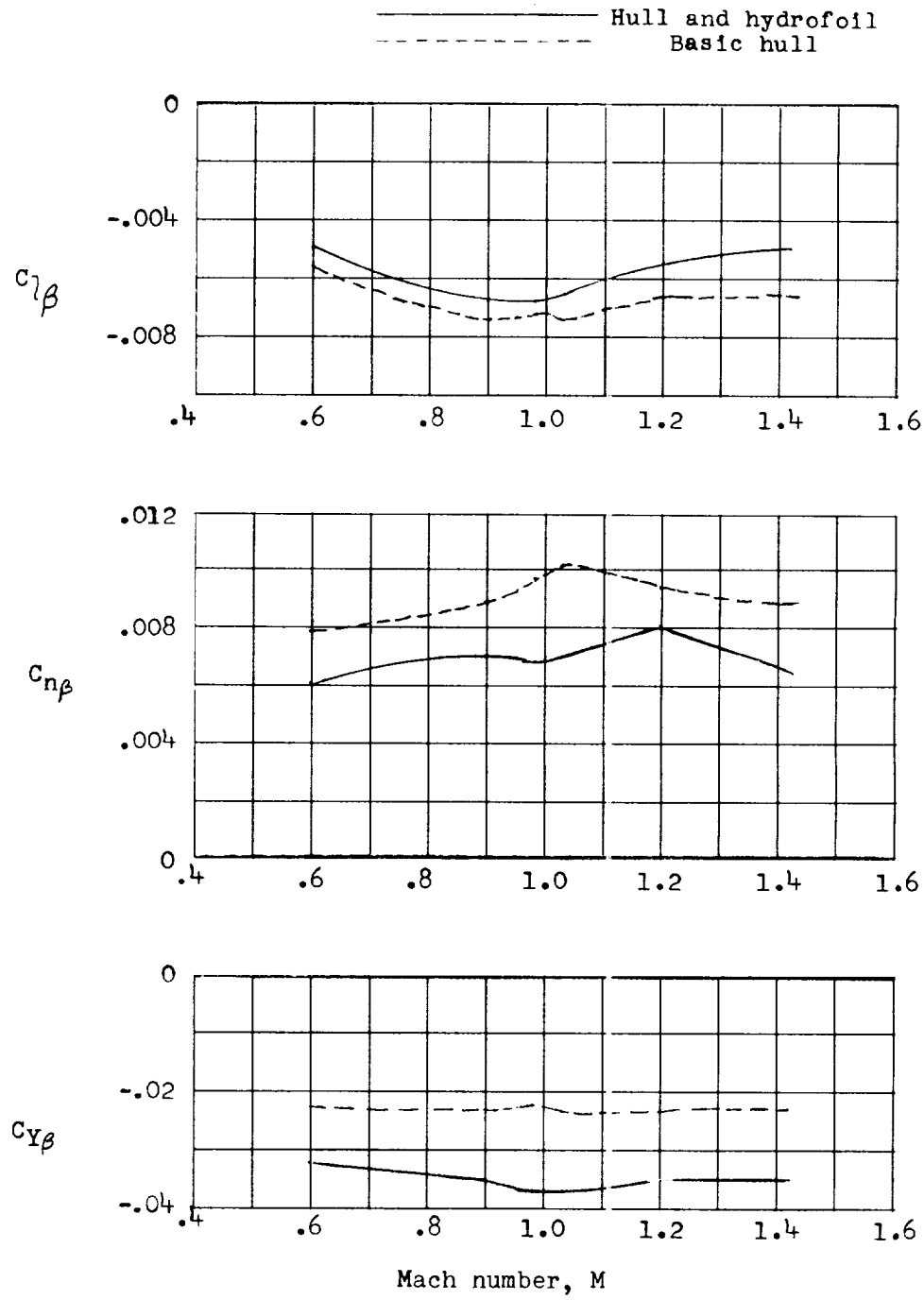

Figure 25.- Summary of lateral stability parameters of hull model with and without hydrofoils. Natural transition; $i_t = -2.5^\circ$; stagnation pressure, 0.5 atmosphere; $\alpha \approx 5^\circ$.